European Journal of Pharmaceutics and Biopharmaceutics 174 (2022) 111–130

Contents lists available at ScienceDirect

European Journal of Pharmaceutics and Biopharmaceutics

journal homepage: www.elsevier.com/locate/ejpb

Host cell targeting of novel antimycobacterial 4-aminosalicylic acid derivatives with tuftsin carrier peptides

Lilla Borbála Horváth [a,b,i], Martin Krátký [c], Václav Pflégr [c], Előd Méhes [d,i], Gergő Gyulai [e], Gergely Kohut [f], Ákos Babiczky [g], Beáta Biri-Kovács [h], Zsuzsa Baranyai [a], Jarmila Vinšová [c], Szilvia Bősze [b,i,*]

[a] ELKH-ELTE Research Group of Peptide Chemistry, Eötvös Loránd Research Network, Eötvös Loránd University, Pázmány Péter sétány 1/A, H-1117 Budapest, Hungary
[b] Hevesy György PhD School of Chemistry, Faculty of Science, Institute of Chemistry, Eötvös Loránd University, Pázmány Péter sétány 1/A, H-1117 Budapest, Hungary
[c] Department of Organic and Bioorganic Chemistry, Faculty of Pharmacy, Charles University, Heyrovského 1203, 500 05 Hradec Králové, Czech Republic
[d] Department of Biological Physics, Eötvös Loránd University, Pázmány Péter sétány 1/A, H-1117 Budapest, Hungary
[e] Laboratory of Interfaces and Nanostructures, Eötvös Loránd University, Pázmány Péter sétány 1/A, H-1117 Budapest, Hungary
[f] Biomolecular Self-assembly Research Group, Institute of Materials and Environmental Chemistry, Research Centre for Natural Sciences, Magyar tudósok körútja 2, H-1117 Budapest, Hungary
[g] Neuronal Network and Behavior Research Group, Institute of Cognitive Neuroscience and Psychology, Research Centre for Natural Sciences, Magyar tudósok körútja 2, H-1117 Budapest, Hungary
[h] Faculty of Science, Institute of Chemistry, Eötvös Loránd University, Pázmány Péter sétány 1/A, H-1117 Budapest, Hungary
[i] National Public Health Center, Albert Flórián út 2-6, H-1097 Budapest, Hungary

ARTICLE INFO

Keywords:
Mycobacterium tuberculosis
Host cell targeted delivery
Antimycobacterial compound
Tuftsin carrier peptides
Neuropilin receptor
N-substituted 4-aminosalicylic acid derivatives

ABSTRACT

Mycobacterium tuberculosis is an intracellular pathogen and the uptake of the antimycobacterial compounds by host cells is limited. Novel antimycobacterials effective against intracellular bacteria are needed. New *N*-substituted derivatives of 4-aminosalicylic acid have been designed and evaluated. To achieve intracellular efficacy and selectivity, these compounds were conjugated to tuftsin peptides *via* oxime or amide bonds. These delivery peptides can target tuftsin- and neuropilin receptor-bearing cells, such as macrophages and various other cells of lung origin. We have demonstrated that the *in vitro* antimycobacterial activity of the 4-aminosalicylic derivatives against *M. tuberculosis* $H_{37}Rv$ was preserved in the peptide conjugates. The free drugs were ineffective on infected cells, but the conjugates were active against the intracellular bacteria and have the selectivity on various types of host cells. The intracellular distribution of the carrier peptides was assessed, and the peptides internalize and display mainly in the cytosol in a concentration-dependent manner. The penetration ability of the most promising carrier peptide OT5 was evaluated using Transwell-inserts and spheroids. The pentapeptide exhibited time- and concentration-dependent penetration across the non-contact monolayers. Also, the pentapeptide has a fair penetration rate towards the center of spheroids formed of EBC-1 cells.

All amino acids were represented by the one-letter code. Abbreviations in peptide chemistry were used as recommended by Jones, 1999 [1].

1. Introduction

Tuberculosis (TB) is an infectious disease caused by the pathogen *Mycobacterium tuberculosis* (*Mtb*). It is one of the ten leading death causes worldwide, and the leading death caused by a single infectious agent. Despite the efforts to stop the spreading of TB disease, in 2019 10 million TB cases were registered and approximately 1.4 million people died from the disease. It is estimated that one-quarter of the world's population is infected with *Mtb*, serving as a reservoir for the disease [2,3]. Spreading of drug-resistant *Mtb* strains is an additional threat. Multidrug-resistant TB (MDR-TB) is defined as resistant to isoniazid and rifampicin, two first-line drugs, extensively drug-resistant TB (XDR-TB) is MDR-TB with additional resistance to fluoroquinolones and any of the second-line injectable agents: amikacin, kanamycin, or capreomycin. In

* Corresponding author at: Pázmány Péter sétány 1/A, Budapest H-1117, Hungary, P.O. Box 32, 1518 Budapest 112, Hungary.
E-mail addresses: lillahorvath@ttk.elte.hu (L. Borbála Horváth), martin.kratky@faf.cuni.cz (M. Krátký), pflergv@faf.cuni.cz (V. Pflégr), elod.mehes@ttk.elte.hu (E. Méhes), gyulai.gergo@ttk.elte.hu (G. Gyulai), kohut.gergely@ttk.mta.hu (G. Kohut), babiczky.akos@ttk.mta.hu (Á. Babiczky), beata.biri-kovacs@ttk.elte.hu (B. Biri-Kovács), baranyaizsuzs@gmail.com (Z. Baranyai), jarmila.vinsova@faf.cuni.cz (J. Vinšová), szilvia.bosze@ttk.elte.hu (S. Bősze).

https://doi.org/10.1016/j.ejpb.2022.03.009
Received 7 September 2021; Received in revised form 8 March 2022; Accepted 24 March 2022
Available online 2 April 2022

Abbreviation

ASA	4-aminosalicylic acid derivative
Boc	*tert*-butyloxycarbonyl protecting group
BMMΦ	murine bone marrow culture-derived macrophages
Cf	5(6)-carboxyfluorescein
CFU	colony forming units
CLSM	confocal laser scanning microscopy
CM	complete medium
CMFDA	5-chloromethylfluorescein diacetate
DBU	1,8-diazabicyclo[5.4.0.]undec-7-ene
DIC	*N,N'*-diisopropylcarbodiimide
DIEA	*N,N*-diisopropylethylamine
DMEM	Dulbecco's Modified Eagle's Medium
DMF	*N,N*-dimethylformamide
DMSO	dimethyl sulfoxide
FBS	fetal bovine serum
Fmoc	9-fluorenylmethyloxycarbonyl protecting group
HOBt	1-hydroxybenzotriazole
HPLC	high performance liquid chromatography
HR-MS	high resolution mass spectrometry
HRP	horseradish peroxidase
IC_{50}	inhibitory concentration
ICM	incomplete medium
MDR-TB	multidrug resistant tuberculosis
MIC	minimal inhibitory concentration
MTT	3-(4,5-dimethylthiazol-2-yl)-2,5-diphenyltetrazolium bromide
Mtb	*Mycobacterium tuberculosis*
NMP	1-methyl-2-pyrrolidone
NRP	neuropilin
OT10	dituftsin derivative, $[TKPKG]_2$
OT5	monotuftsin derivative, TKPKG
PBS	phosphate buffered saline
PFA	paraformaldehyde
RPMI-1640	Roswell Park Memorial Institute 1640 medium
R_t	retention time
SI	selectivity index
^{t}Bu	*tert*-butyl protecting group
TB	tuberculosis
TDR-TB	totally drug resistant tuberculosis
TFA	trifluoroacetic acid
TIS	triisopropylsilane
UC_{50}	uptake concentration
XDR-TB	extensively drug resistant tuberculosis

the past few years, totally drug-resistant TB (TDR-TB) cases were registered, which are resistant to all available TB drugs [4]. Consequently, there is a huge need to develop new antimycobacterial agents.

Salicylanilide derivatives have various biological effects. Their antimicrobial, antifungal, antihelmintic [5], antiprotozoal [6], and antitumor [7,8] activities have been reported. Salicylanilide derivatives inhibit the two-component regulatory system of bacteria [9,10], the isocitrate lyase enzyme [11–15], they are selective inhibitors of interleukin 12p40 [16,17] and as proton shuttles, these compounds can destroy the cellular proton gradient [18,19]. 4-aminosalicylic acid (*para*-aminosalicylic acid, ASA) is a well-known second-line antimycobacterial compound that is used clinically in the treatment of MDR-TB. This compound is a prodrug, targeting the essential folate metabolism in *Mtb* [20,21]. Tetrahydrofolate - a one-carbon unit donor in many biosynthetic pathways – is synthesized *de novo* in most microorganisms, thus in *Mtb* too. This makes folic acid biosynthesis an attractive antimicrobial drug target [22].

Mtb can survive inside host cells to hide from the immune system, survive (in active or latent forms over prolonged periods), and even spread [23]. *Mtb* mainly reside in phagocytic cells, but they also find their way into non-phagocytic cells (epithelial and squamous cells of the lung, etc.). The host cells are not only primarily infected but also act as a 'reservoir' for pathogens that could seed in other tissues, leading to systemic infections. *Mtb* also can invade and localize inside various host cells (both professional immune cells as macrophages or non-professionals like epithelial and endothelial cells of the lung and other organs etc.) [24–26].

Mycobacteria possess an unusual and complex cell wall dominated by lipids and carbohydrates that provides a permeability barrier against drugs (is thought to contribute to the intrinsic drug resistance of mycobacteria) and is crucial for their survival, virulence, and dormancy [27,28].

The interaction between drugs and the host cell membrane/pathogen cell wall plays a fundamental role in the pharmacokinetics of the compound and lipophilic compounds possess remarkable inhibition activity on mycobacterial cultures. Therefore, mainly more than half of effective new candidates exhibit low solubility and selectivity in target cells, the increase of solubility, selectivity, and bioavailability is essential.

To achieve the higher solubility, selectivity, internalization rate, and intracellular efficacy of the antimycobacterial compounds, different delivery vehicles can be used. Targeting peptides can enhance cellular uptake of active agents *via* receptor-mediated endocytosis, thus, peptide-based drug conjugates can increase the intracellular efficacy of antimycobacterial compounds [29–36]. The development of delivery peptides is also a demanding process (solubility, efficient targeting, and stability as well as cytotoxicity aspects). Due to the limited number of receptor sites and specific cell surface molecules on infected cells, host cell-targeted peptide-based delivery is an attractive approach for bioactive compounds with narrow therapeutic windows and/or active at very low concentrations [37]. The need for intracellular delivery of the effective antimycobacterial compounds has been recognized for many years: the challenge is to design the adequate delivery peptides to shuttle an antimycobacterial agent in a conjugated form that can be internalized by host cells and then released into these cells in an active form. The distribution of a compound in the host cells is mainly a function of its physicochemical properties. The conjugation to a carrier peptide will modify the chemical character of the antimycobacterial compound to achieve effective internalization and controlled release in the infected host cells. In our previous study, we have presented that the physicochemical properties of the delivery peptides can be tuned by altering their composition and attachment of the targeted active compounds [32,33,35,36,38]. We have also proved that receptor-mediated endocytosis can enhance the internalization of active compounds such as peptide conjugated antimycobacterial agents. Receptors with peptide ligands that are expressed mainly on *Mtb* host cells (mainly macrophages) could be targets to deliver active compounds. Tuftsin receptor is a well-known target for macrophage and monocytes-directed delivery [30,32,39–43]. Tuftsin-based peptide derivatives are promising carriers, and these peptides are ligands of the neuropilin (NRP) receptors, and they have immunostimulatory and phagocytosis stimulating activity.

NRPs are single-pass transmembrane glycoprotein co-receptors with numerous binding partners, they enhance responses to growth factors such as vascular endothelial growth factor, hepatocyte growth factor, platelet-derived growth factor, and fibroblast growth factor [44,45]. NRPs mediate their cellular response *via* several signaling pathways; tuftsin binding to NRP receptors activates the transforming growth factor-beta pathway [46]. NRPs have a role in neuronal guidance, cardiovascular development, cell migration, lung development, and several

immune functions [47–50]. In the immune system, NRPs are present in T-cell activation, dendritic cell, and monocyte maturation [48,51]. NRPs are present in alveolar and bronchial macrophages, and upon pathological conditions such as inflammation or lung cancer increased NRP content is observed [52]. Targeting NRPs in lung diseases is a novel option [53–55]. NRPs have known receptors for tuftsin peptides; the tuftsin derivative TKPPR binds to NRP-1 with higher affinity than to NRP-2 [56]. The most promising tuftsin derivatives contain the CendR motif (R/KXXR/K), which can be essential for binding to the b1/b2 domain of NRP-1 [51,57].

Tuftsin (human: TKPR, canine: TKPK) is a natural tetrapeptide from the CH2 domain of IgG produced by enzymatic cleavage [58,59]. Tuftsin possesses immunostimulatory, chemotaxis, and phagocytosis activating, antitumor properties and is nontoxic to animals and humans [60]. Tuftsin is taken up by macrophages and polymorphonuclear phagocytes *via* receptor-mediated endocytosis [39,40,43]. Due to the wide spectrum of biological activities, tuftsin and its derivatives have been in the scope of numerous examinations in the last decades [61].

In our research group, a series of sequential oligopeptides based on the canine tuftsin peptide have been developed in the last fifteen years [62]. These peptides with the sequence $[TKPKG]_n$, (n = 1, 2, 3, 4) have tuftsin-like properties and can be used as delivery systems to target tumor cells [63] and the main host cells of *Mtb*, macrophages [32–34,36,64]. Based on previous studies, conjugates containing monotuftsin delivery peptides (TKPKG, TKPR, TKPPR) are more effective against extracellular and intracellular *Mtb* with lower cytotoxicity to host MonoMac6 cells. Fatty acid-containing derivatives have increased lipophilic character [36].

For the release of the compounds, enzyme-labile linker sequences (GFLG, GFYA) were built between the carrier sequences and the salicylanilide derivatives. The tetrapeptide sequences can be cleaved by cathepsin B, a lysosomal cysteine protease [65,66].

Three-dimensional cell cultures (spheroids etc.) more accurately model physiological cellular functions and cell-to-cell interactions than two-dimensional monolayers [67]. The spheroids composed from cells of lung origin are suitable and simple objects to characterize the penetration ability of the delivery peptides and their drug-conjugates.

Physical barriers limit the efficacy of active compounds and delivery peptides. To comparatively estimate penetration ability *via* tissue barriers Transwell arrangements are promising models [68,69]. To establish a simple *in vitro* model of the bronchial and alveolar barriers, we have employed Transwell inserts with non-contact, submerged co-cultured monolayers to compare the trafficking of the tuftsin peptides.

In this study, three novel 4-aminosalicylic acid derivatives (ASA) with remarkable antimicrobial activity were designed and characterized. These active compounds were conjugated to NRP receptor-ligand oligotuftsin peptide carriers ($[TKPKG]_n$, (n = 1, 2)) *via* amide an oxime bond. Enzyme-labile linker sequences (GFLG, GFYA) were built between the ASA derivatives and the carrier peptides to assist the release of the active compounds. The *in vitro* antimycobacterial efficacy on the intracellular population of the bacteria was assessed. The cellular uptake, intracellular localization, and lysosomal degradation pattern were also evaluated. The *in vitro* penetration ability of the carrier peptide TKPKG was determined using spheroids as the tissue-mimicking cellular environment as well as tissue barrier model.

2. Results and discussion

2.1. Design and synthesis of 4-aminosalicylic acid (ASA) derivatives

Three novel 4-aminosalicylic acid derivatives, namely: methyl 4-[3-(4-acetylphenyl)ureido]-2-hydroxybenzoate (**ASA1**), 4-[3-(4-acetylphenyl)ureido]-2-hydroxybenzoic acid (**ASA2**) and [3-hydroxy-4-(methoxycarbonyl)phenyl]glycine (**ASA3**) were designed, synthesized (Scheme 1) and characterized. ASA1 and ASA2 were synthesized with the reaction between 4-acetylphenyl isocyanate and methyl 4-aminosalicylate or 4-aminosalicylic acid, respectively (Scheme 1). These compounds contain carbonyl groups which can be used for conjugation *via* oxime bonds (Scheme 2B). ASA3 was obtained from the reaction of methyl 4-aminosalicylate and glyoxylic acid (Scheme 1). ASA3 contains a carboxyl group that can be used for conjugation *via* an amide bond (Scheme 2A). Detailed synthesis routes and chemical (thin layer chromatography, TLC; melting point, elemental analysis, Fourier-transform infrared spectroscopy, FT-IR; mass spectrometry) and structural (nuclear magnetic resonance, NMR spectroscopy) characterization of the novel compounds are described in the Supplementary Material. Analytical chromatograms and mass spectra of ASA1, ASA2, and ASA3 are shown in the Supplementary material (SF1-3).

2.2. Synthesis of the peptide carriers and their fluorescent derivatives

In this study $[TKPKG]_n$, n = 1, 2 (OT5 and OT10) derivatives were selected as delivery peptides [36]. For the liberation of the active ASA compounds, we have designed conjugates in which the tuftsin carrier was coupled *via* tetrapeptide sequences (GFLG and GFYA) susceptible to cleavage catalyzed by lysosomal enzymes [65,70,71]. Six different

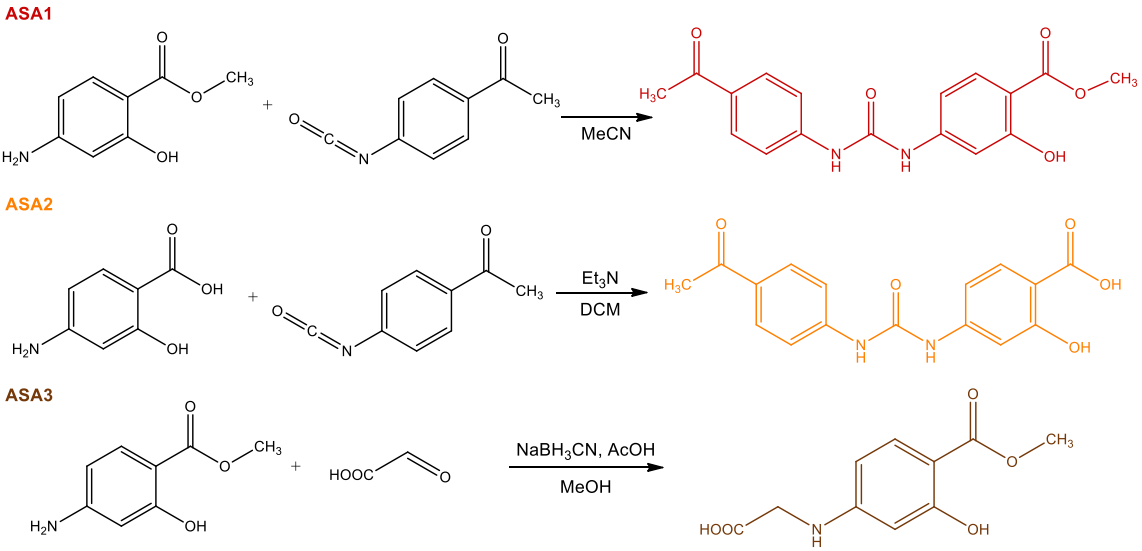

Scheme 1. Synthesis of 4-aminosalicylic acid (ASA) derivatives.

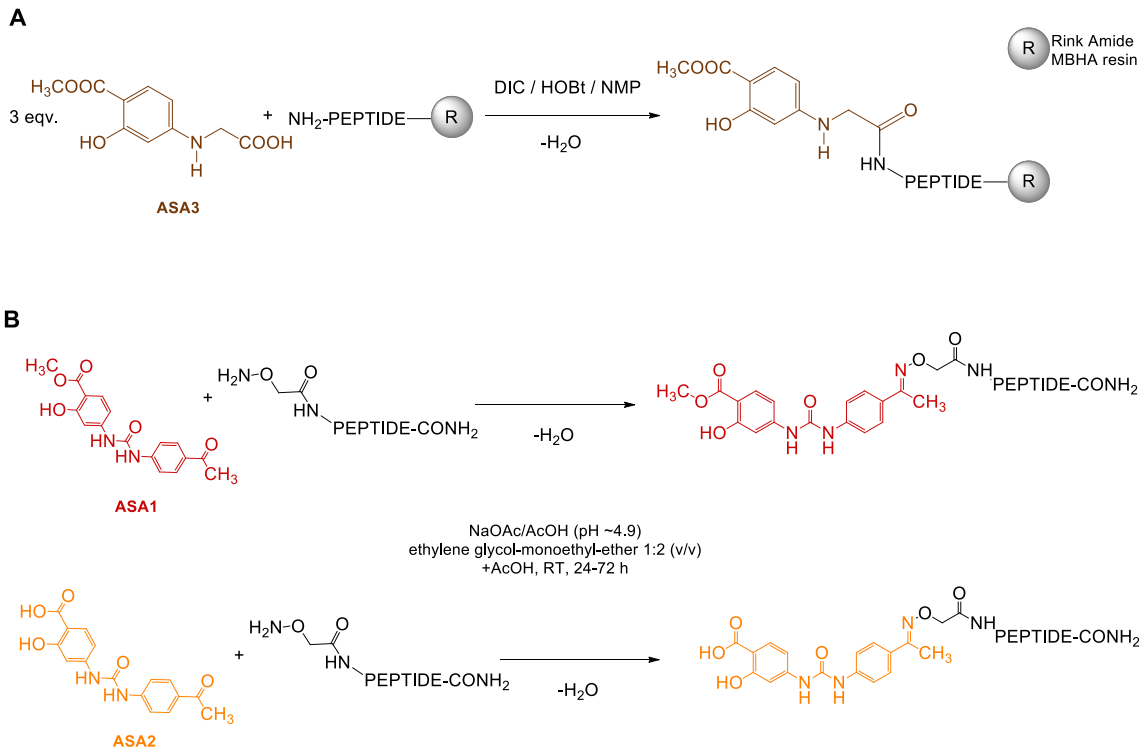

Scheme 2. Conjugation of ASA derivatives to peptide carriers. Amide bond was formed on resin between ASA3 and tuftsin delivery peptides (**A**), conjugation between ASA1 or ASA2, and cleaved, crude (aminooxy)acetylated tuftsin peptides with the formation of oxime bond (**B**).

peptide sequences were applied and compared regarding the number of tuftsin units, and the presence and sequence of the linker.

Peptides were synthesized using standard Fmoc/^{t}Bu strategy with an identical method as in Baranyai *et al.* [36]. Scheme 3 illustrates the process of peptide synthesis. All peptides have the *C*-terminal in amide form. In all cases, acetylated (Ac-), 5(6)-carboxyfluorescein (Cf-), and (aminooxy)acetylated (Aoa-) peptide derivatives have been synthesized. Peptides were cleaved from the resin with trifluoroacetic acid (TFA) in the presence of appropriate scavengers. Crude Aoa-peptide derivatives were used for conjugation by forming an oxime bond. Ac-peptides were used in selectivity studies on human cell cultures modeling host cells of *Mtb*. Cf-peptide derivatives were purified using an HPLC system with a semi-preparative reverse phase column and were used in *in vitro* cellular uptake and intracellular localization studies. All tuftsin delivery peptides were chemically characterized using analytical HPLC with reversed-phase column and high-resolution mass spectrometry (HR-MS). Supplementary Table 1. (ST1) summarizes the chemical characterization of Ac- and Cf-peptide derivatives. Analytical chromatograms

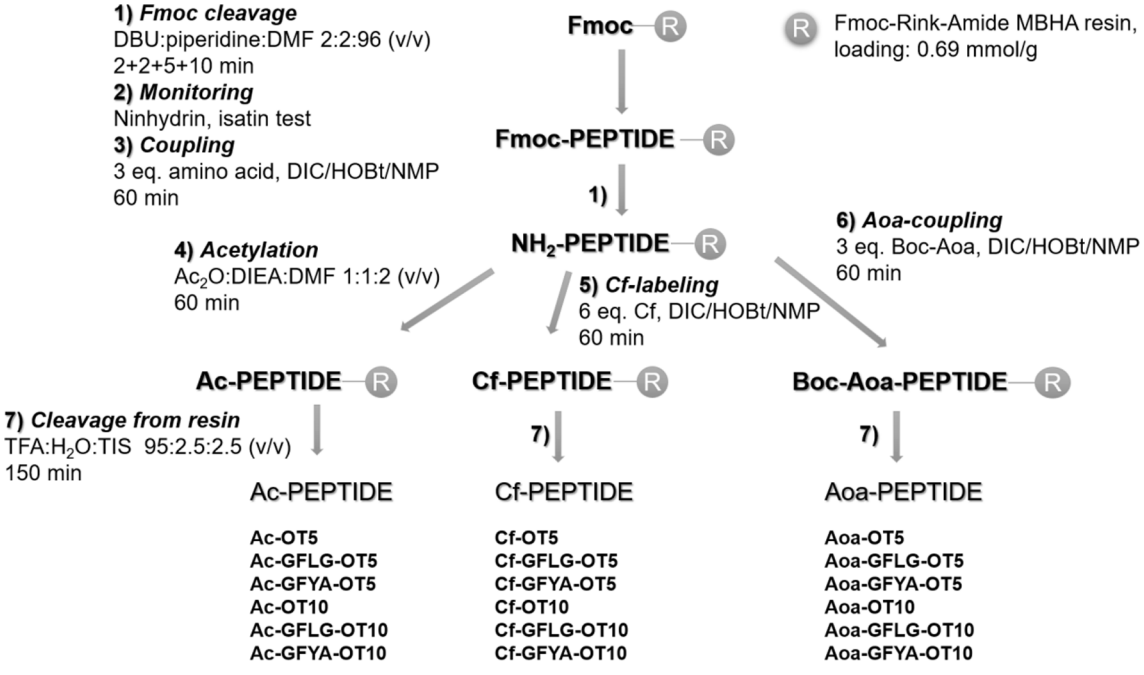

Scheme 3. Synthesis of tuftsin delivery peptides using Fmoc/^{t}Bu strategy.

and mass spectra are presented in the Supplementary Material (SF3-15). Amino acid composition and peptide content were determined using amino acid analysis. Data extracted from the amino acid analysis are presented in Supplementary Material ST2.

2.3. Synthesis and chemical characterization of conjugates

In this study, eighteen novel ASA-conjugates as antimycobacterial compound candidates containing amide and oxime bonds were designed, synthesized, and chemically characterized.

Amide bonds between the free compound and the tuftsin delivery peptides were formed on the resin (Scheme 2A). Conjugates were cleaved from the resin with TFA in the presence of appropriate scavengers. Oxime bonds between the free compounds and the tuftsin delivery peptides were formed in the liquid phase, under acidic conditions (Scheme 2B).

Conjugates were chemically characterized using analytical HPLC with reversed-phase column and high-resolution mass spectrometry (Table 1). All conjugates are homogenous with appropriate mass accuracy. Analytical chromatograms and mass spectra are presented in the Supplementary Material (SF28-45).

2.4. Lipophilicity profile of free compounds and tuftsin conjugates

Lipophilicity is a parameter influencing the interaction between the antimycobacterial compounds and membrane structures of the cells (including bacterial and host cell membranes). Log*P* values of free compounds (ASA1, ASA2, ASA3), peptide derivatives, and conjugates were also calculated using the ChemAxonPASS platform (for details see: SF46C). Lipophilicity of free compounds and peptide conjugates can be estimated and compared based on the retention times (R_t) on HPLC systems with C18 columns [36,72–74]. The more hydrophobic a compound is, the stronger its retention on the column. This method can be applied in the case of structurally similar compounds, using the same gradient. Table 1 summarizes the retention times of the free compounds and the conjugates. Tuftsin peptides possess Thr and Lys amino acids, therefore they have high hydrophilic character. Free compounds (ASA1, ASA2, and ASA3) have longer retention and higher log*P* values in comparison with their conjugates. Lipophilicity is essential for the antimicrobial activity (see Fig. 1A), but the cellular uptake and bioavailability are limited. The conjugation of the ASA moieties to tuftsins made the conjugates more lipophilic than the tuftsin itself. Conjugate with the GFLG or GFYA spacer built up by non-polar amino acids has more lipophilic character than its analog without the spacer region.

ASA1 is the most lipophilic and ASA3 is the least lipophilic free compound. In the case of the conjugates, the ASA1 derivatives are the most lipophilic, and OT5 and OT10 tuftsin delivery peptides have smaller retention times and log*P* values in comparison with the GFLG and GFYA linker containing derivatives. Conjugates containing OT10 peptides are the least lipophilic, and GFLG linkers containing conjugates are the most lipophilic ones. The tendencies are similar based on the retention times and calculated logP values (SF46A, C), respectively. Calculated logP values plotted against retention times are presented in Supplementary Material SF47. The lipophilic character of a compound can affect its efficacy against extracellular and intracellular bacteria. SF46B illustrates the retention times and efficacy of ASA compounds and conjugates. The most hydrophilic conjugates have the highest inhibitory effect against bacteria.

2.5. Stability of the conjugates under different assay conditions

For the determination of antimycobacterial activity, free compounds and conjugates were dissolved in DMSO. As the length of the measurements is 4–5 weeks, the conjugates must be stable under the conditions used. The stability of the conjugates in DMSO solution at 37 °C was tested using an analytical HPLC with a reverse-phase column. In all cases, no degradation of conjugates could be observed for up to 31 days.

Table 1
Chemical characterization of the conjugates.

Code*	log*P*[a]	$M_{av\ (calc)}$[b]	$M^c_{mono\ (calc)}$	meas. m/z[d]	calc. m/z[e]	ppm[f]	R_t (min)[g]
ASA1	3.0	328.3193	328.1059	329.1129	329.1132	−0.9	18.1
ASA1-Aoa-OT5	−2.9	912.0002	911.4501	912.4578	912.4574	0.5	15.4
ASA1-Aoa-GFLG-OT5	−3.2	1286.4344	1285.6455	1286.6528	1286.6528	0.0	16.8
ASA1-Aoa-GFYA-OT5	−3.0	1350.4766	1349.6404	675.8270	675.8275	−0.7	16.4
ASA1-Aoa-OT10	−7.1	1423.6152	1422.7619	1423.7683	1423.7692	−0.6	14.8
ASA1-Aoa-GFLG-OT10	−7.4	1798.0493	1796.9574	599.9923	599.9931	−1.3	16.2
ASA1-Aoa-GFYA-OT10	−7.4	1862.0915	1860.9523	466.2453	466.2454	−0.1	15.9
ASA2	2.7	314.2928	314.0903	315.0971	315.0976	−1.5	16.2
ASA2-Aoa-OT5	−4.7	897.9737	897.4345	449.7241	449.7245	−1.0	14.4
ASA2-Aoa-GFLG-OT5	−5.1	1272.4078	1271.6299	1272.6356	1272.6372	−1.2	15.7
ASA2-Aoa-GFYA-OT5	−5.0	1336.4500	1335.6248	668.8189	668.8197	−1.2	15.4
ASA2-Aoa-OT10	−8.8	1409.5886	1408.7463	470.5891	470.5894	−0.6	14.2
ASA2-Aoa-GFLG-OT10	−9.2	1784.0227	1782.9417	595.3207	595.3212	−0.8	15.2
ASA2-Aoa-GFYA-OT10	−9.4	1848.0649	1846.9366	462.7412	462.7414	−0.5	15.0
ASA3	1.3	225.1980	225.0637	226.0709	226.0710	−0.4	15.4
ASA3-OT5	−4.4	735.8282	735.3915	736.3987	736.3988	−0.1	13.4
ASA3-GFLG-OT5	−4.8	1110.2624	1109.5869	1110.5938	1110.5942	−0.3	15.1
ASA3-GFYA-OT5	−4.5	1174.3046	1173.5819	587.7980	587.7982	−0.4	14.8
ASA3-OT10	−8.4	1247.4432	1246.7034	1247.7108	1247.7107	0.1	13.0
ASA3-GFLG-OT10	−8.8	1621.8873	1620.8988	811.4562	811.4567	−0.6	14.6
ASA3-GFYA-OT10	−8.9	1685.9195	1684.8937	562.6380	562.6385	−0.9	14.4

[a] Calculated log*P* values were obtained by ChemAxonPASS online platform.
[b] Average and [c] monoisotopic masses were calculated using CS ChemOffice Pro ver. 12.0 (PerkinElmer Informatics).
[d] For the high-resolution mass spectrometry Q Exactive Focus Hybrid Quadrupole-Orbitrap Mass Spectrometer was used. Data were evaluated using Thermo Scientific Xcalibur software.
[e] $[M_{mono}+(z \times 1.00728)]/z$.
[f] (measured *m/z*-calculated *m/z*)/ calculated $m/z \times 10^6$.
[g] Retention times were determined with Exformma EX1600 analytical HPLC system with YMC-Pack ODS-A C_{18} (100 Å, 4.6 × 150 mm) column. Gradient: 0–5 min 0% B, 5–15 min 0–60% B, 15–25 min 60–100% B, flow rate: 1 mL/min, detector: λ = 220 nm. Eluent A is distilled water with 0.1% TFA (v/v) and eluent B is acetonitrile:water = 80:20 (v/v) with 0.1% TFA.
* The amino acid sequences of the peptides: OT5: TKPKG; OT10: TKPKGTKPKG.

A

Code	*Mtb* H_{37}Rv		
	MIC		
	γ (μg/mL)	μM	CFU
ASA2	0.5	1.6	5
ASA3	1	4.4	8
ASA1	40	121.8	24
ASA2-Aoa-OT5	5	5.6	7
ASA1-Aoa-OT5	20	22.0	3
ASA3-OT5	20	27.2	2
ASA2-Aoa-GFLG-OT5	20	15.7	6
ASA3-GFLG-OT5	20	18.0	40
ASA1-Aoa-GFLG-OT5	40	31.1	14
ASA2-Aoa-GFYA-OT5	15	11.2	12
ASA3-GFYA-OT5	40	34.1	10
ASA1-Aoa-GFYA-OT5	60	44.5	4
ASA2-Aoa-OT10	20	14.2	12
ASA3-OT10	20	16.0	1
ASA1-Aoa-OT10	120	84.3	1
ASA2-Aoa-GFLG-OT10	20	11.2	16
ASA3-GFLG-OT10	60	37.0	33
ASA1-Aoa-GFLG-OT10	80	59.3	8
ASA2-Aoa-GFYA-OT10	15	8.1	16
ASA3-GFYA-OT10	80	47.5	4
ASA1-Aoa-GFYA-OT10	80	62.2	28

B

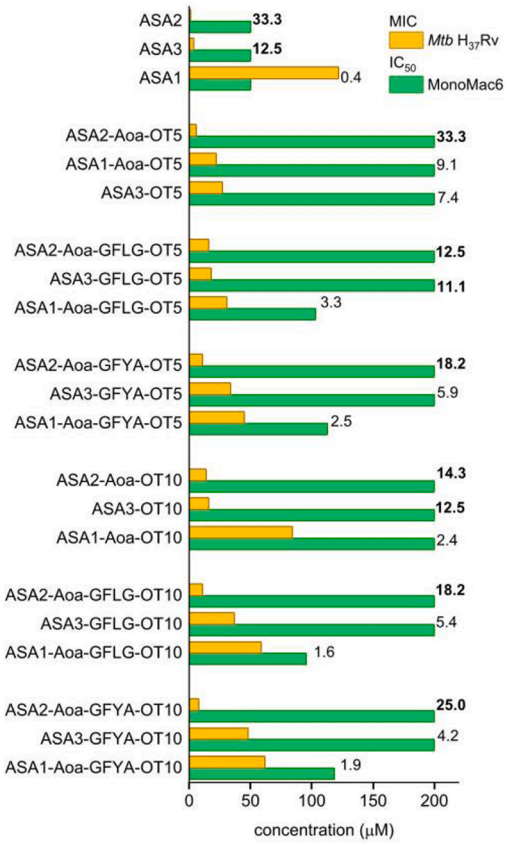

Fig. 1. Antimycobacterial activity of the free compounds and their peptide conjugates was determined on *Mtb* H_{37}Rv cultures (**A**). Selectivity of the compounds was measured on MonoMac6 cells by MTT assay (**B**).

Analytical chromatograms are presented in the Supplementary Material (SF48-65).

For the *in vitro* selectivity studies, free compounds and conjugates were dissolved in an incomplete cell culture medium (ICM). Stability of the conjugates in cell culture medium (RPMI-1640 / DMEM, data not shown) containing 2.5% FBS was tested. In most cases, no significant degradation of conjugates could be observed for up to 24 h. Analytical chromatograms are presented in the Supplementary Material (SF66-82).

2.6. *In vitro antimycobacterial effect of the compounds*

In vitro antimycobacterial activity of the free compounds and the conjugates was determined on *Mtb* H_{37}Rv strain (ATCC 27294) using the conventional broth dilution method (Fig. 1A). Free compounds inhibit the growth of the bacteria and this antimycobacterial effect is preserved after conjugation. ASA2 (0.5 μg/mL, 1.5 μM) has lower minimal inhibitory concentration (MIC) value than ASA3 (1 μg/mL, 4 μM) and ASA1 (40 μg/mL, 122 μM). ASA1-Aoa-OT5 (20 μg/mL, 22 μM) and ASA1-Aoa-GFLG-OT5 (40 μg/mL, 31 μM) have lower MIC than ASA1. Overall, ASA2 derivatives have the lowest MIC values, followed by ASA3 derivatives.

2.7. *Determination in vitro selectivity of the compounds on host cell cultures*

For the *in vitro* selectivity evaluation, different human cell cultures were selected, namely MonoMac6 (model for the main host cells the macrophages and monocytes). As macrophage-independent models for host cells different human lung originated cultures as EBC-1, H838, CALU-1, A549, and LCLC-103H were chosen. Epithelial and squamous-cell aggregates are common within the lung tissue associated with *Mtb* infection. *Mtb* infected host cells (mainly the macrophages and other lung tissue cells) play a pivotal role in chronic-tuberculosis-induced DNA damage, proliferative activities, etc. The infection caused mainly by proliferative changes in the lung tissue (mainly in bronchial and alveolar mucosa) that *Mtb* leaves behind cannot be ignored [75,76]. Therefore, epithelial (originated from bronchial and alveolar airways), squamous and large cell lung carcinoma cells can be utilized to investigate the main features of the carrier peptides.

We have also investigated the *in vitro* selectivity of the free compounds, carrier peptides, and conjugates on human hepatocellular carcinoma cells (HepG2) [36,77–81]. The HepG2 cells represent a simple *in vitro* model for hepatotoxicity. The *in vitro* cytotoxic activity of a representative compound set was also determined on murine bone marrow culture-derived macrophages (BMMΦ) [78,82–85], which cells are considered as murine models of the macrophages and these data are essential before animal experiments.

The *in vitro* selectivity was determined on human cell cultures assessing the cytostatic effect of the delivery peptides as Ac-derivatives, ASA compounds, and conjugates. The cytostatic activity was determined by end-point MTT assay on MonoMac6, EBC-1, H838, and CALU-1 cell cultures (SF83). On MonoMac6 monocyte cells, ASA derivatives and Ac-peptides have no cytostatic effect up to 50 μM and to 200 μM, respectively. Except for ASA1-Aoa-GFLG-OT5 (selectivity index, SI: 3.3), ASA1-Aoa-GFYA-OT5 (SI: 2.5), and ASA1-Aoa-GFLG-OT10 (SI: 1.6) conjugates also have no cytostatic effect (Fig. 1B).

ASA compounds, Ac-peptides, and most conjugates are selective on EBC-1 lung cells. ASA1-Aoa-GFLG-OT5 has a slight cytostatic effect (SI: 2.8).

On H838 cells, the selectivity of ASA compounds, Ac-peptides, and conjugates was observed. ASA1-Aoa-GFLG-OT5 (SI: 3.2) and ASA1-Aoa-GFLG-OT10 (SI: 2.3) have a moderate cytostatic effect. On CALU-1 cells

Ac-peptides have no, but ASA1 has a moderate cytostatic effect. Interestingly, some conjugates have remarkable cytostatic effects on CALU-1 cells, such as ASA1-Aoa-GFLG-OT5 (SI: 1.4) and ASA3-OT10 (SI: 3.2).

The compounds were also selective on A549 cell culture, as presented in the Supplementary Material (SF84 and ST3).

The selectivity of the compounds was also determined by HepG2 cell culture (SF84 and ST3). *In vitro* cytotoxic activity of selected compounds was determined on murine bone marrow-derived macrophages (BMMΦ). Inhibitory concentration (IC_{50}) values are summarized in Supplementary Material ST4.

Based on the selectivity indexes, ASA2 and ASA3 are promising candidates as antimycobacterial agents. ASA1 itself has low selectivity (SI: 0.4), however, its peptide conjugates have increased selectivity (ASA1-Aoa-OT5 SI: 9.1) both on host cells and hepatocytes. ASA2 and its conjugates were not cytostatic, and a high selectivity was determined (ASA2 SI: 33.3, ASA2-Aoa-OT5 SI: 33.3). In the case of ASA3 peptide conjugates (ASA3-OT5 SI: 7.4), the host cell selectivity is slightly decreased in comparison with the free compound (ASA3 SI: 12.5). Selectivity indexes are summarized in Supplementary Material SF84.

2.8. Membrane integrity studies using atomic force microscopy

The membrane integrity was assessed following treatment with ASA derivatives and their OT5 conjugates on MonoMac6 and (Fig. 2A, B) and EBC-1 (Fig. 2C, D) cells. The morphology of a cell is closely related to its viability and its functions. When a cell's viability changes, its surface morphology changes. The surface morphology of the fixed cells was investigated with atomic force microscopy (AFM). Representative images of the native and treated cells are summarized in Fig. 2B and D.

Scale-dependent surface roughness of the cells was determined according to Antonio et al [86]. Roughness parameters were calculated for individual line-profiles using different high-pass cut-off frequencies in the normalized range of 0 to 0.3, where 1 is the Nyquist frequency. As the cut-off frequency has increased a decrease in the root mean square roughness (R_q) can be observed. At certain cut-off frequencies, a change in the slope of the R_q values corresponds to the filtration of surface information. This can be more sensitively followed by plotting the profile skewness (R_{sk}) as a function of the cut-off frequency. The characteristic cut-off frequencies can be identified with the zero-line cross-overs of the R_{sk} values. Representative images and surface roughness of EBC-1 cells treated with ASA derivatives and Ac-OT5 are presented in the Supplementary Material SF86.

The changes in the surface roughness values then translate to an overall change in the cellular morphology in the case of 500 nm cut-off wavelength, a change in the fine structure of the cell for the 200 nm cut-off, and molecular changes in the cellular membrane for the 100 nm cut-off. R_q values and their 95% confidence intervals were determined from 30 line-profiles for each sample (Fig. 2A and C).

The membrane integrity of the different cells was preserved after treatment with peptide conjugates according to the surface roughness and root mean square roughness data.

The graphs representing the MonoMac6 (Fig. 2A), and EBC-1 (Fig. 2C) cells surface morphology and the extracted data suggest that the ASA conjugates do not influence the membrane integrity. EBC-1 cells were also treated with ASA derivatives and the carrier peptide Ac-OT5. The non-conjugated ASA compounds slightly have altered cell morphology and the rate of the membrane damaged cells is increased.

A typical skewness plot can be seen in the Supplementary Material SF87A. Three characteristic cut-off frequencies were found around 0.015–0.016, 0.035–0.045, and 0.07–0.09 ranges. As such for the comparative analysis of the scale-dependent surface roughness 0.0158, 0.039, and 0.078 cut-off frequencies were chosen corresponding with real-space wavelengths of 500 nm, 200 nm, and 100 nm. Example line-profiles and their corresponding roughness profiles at the selected cut-off frequencies are shown in the Supplementary Material SF87B.

BMMΦ cells were also treated with ASA1-Aoa-OT5, ASA2-Aoa-OT5, and ASA3-OT5 conjugates. Representative images and surface roughness are presented in SF88.

2.9. Cellular internalization and localization of Cf-peptides

In vitro cellular uptake of Cf-peptides was determined using flow cytometry. Cellular uptake can be compared based on the measured intracellular fluorescence intensity. The internalization ability of the Cf-peptides was studied at the 6.25–50 μM concentration range. The *in vitro* cytotoxicity of Cf-peptides was also evaluated during the analysis. In comparison with the untreated control, Cf-peptides have no cytotoxic effect. The percentage of live cells was determined and presented in Supplementary Material SF85. Flow cytometry measurements revealed a concentration-dependent internalization of the Cf-tuftsin peptides

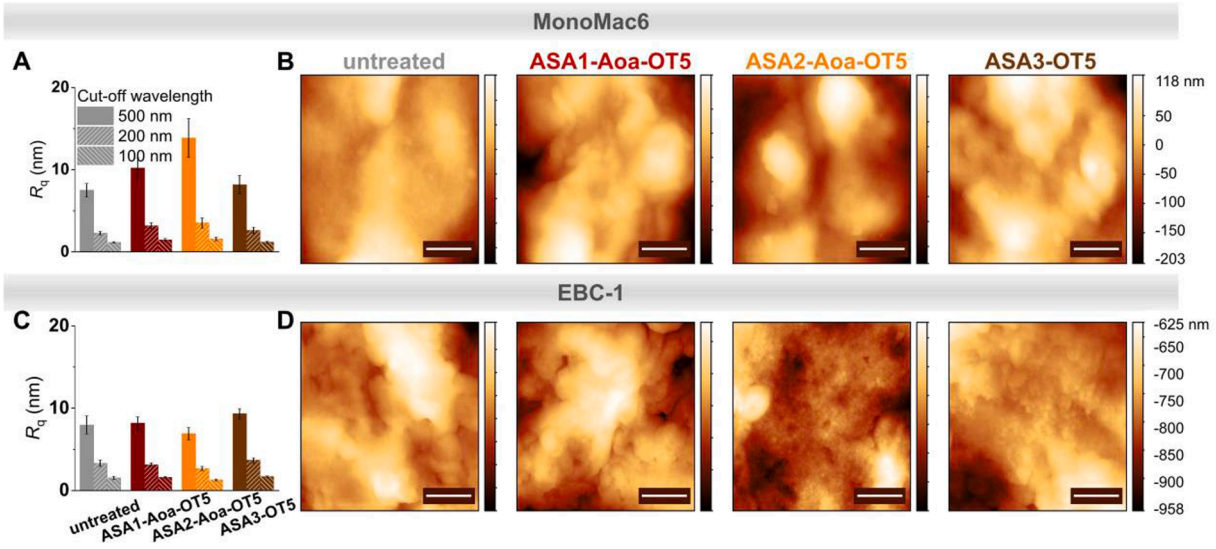

Fig. 2. Membrane integrity studies of MonoMac6 (**A**, **B**) and EBC-1 (**C**, **D**) cells. Average root mean square roughness values of MonoMac6 (**A**) and EBC-1 (**C**) cells at different cut-off frequencies. The error bars represent 95% confidence intervals. High-resolution morphology images of MonoMac6 (**B**) and EBC-1 (**D**) cells before and after treatments. The apex area of the cells was selected for imaging with a scan area of 2 μm × 2 μm (512 × 512-pixel resolution), where the cellular curvature has the smallest distortion effect on the recorded height profiles. Scale bar represents 500 nm.

(SF100-103). Different Cf-tuftsin peptides showed similar internalization profiles. Calculated UC_{50} values (the interpolated concentration required for intracellular fluorescence in 50% of the cell [87] are summarized in Fig. 3A. Cf-OT5 (9.95 μM) has the lowest UC_{50} value, the highest cellular uptake rate on MonoMac6 cells. Cf-GFYA-OT10 (UC_{50} = 18.36 μM) has the lowest uptake (Fig. 3B). The intracellular fluorescence intensities and time-dependent cellular uptake of Cf-peptides on MonoMac6 cells are presented in the Supplementary Material SF100.

To visualize the subcellular localization of the Cf-peptides confocal microscopy images were captured (CLSM images of MonoMac6 cells treated (25 μM, 3 h) are presented in Fig. 3C and the Supplementary Material SF104, SF105). Peptide Cf-OT5 showed diffuse intracellular distribution, while in the case of Cf-OT10, mainly vesicular localization was captured (SF105). Besides cytoplasmic localization Cf-OT10 showed co-localization with lysosomal staining, possibly indicating that this compound internalizes not only through the *endo*-lysosomal pathway, but also through direct cell penetration. Therefore, the majority of Cf-OT10 can be trapped in endosomal compartments. Subsequently, any conjugated cargo might be trapped, as well. Significantly lower intracellular antimycobacterial activity of ASA-OT10 conjugates (Fig. 4A)

A

Cf-peptide	UC_{50} (μM)			
	MonoMac6	EBC-1	H838	CALU-1
Cf-OT5	9.95	9.31	32.93	28.06
Cf-GFLG-OT5	14.53	32.48	>50	26.32
Cf-GFYA-OT5	17.23	>50	>50	15.00
Cf-OT10	11.44	8.75	26.56	24.46
Cf-GFLG-OT10	12.57	23.08	39.33	19.73
Cf-GFYA-OT10	18.36	37.38	>50	27.05

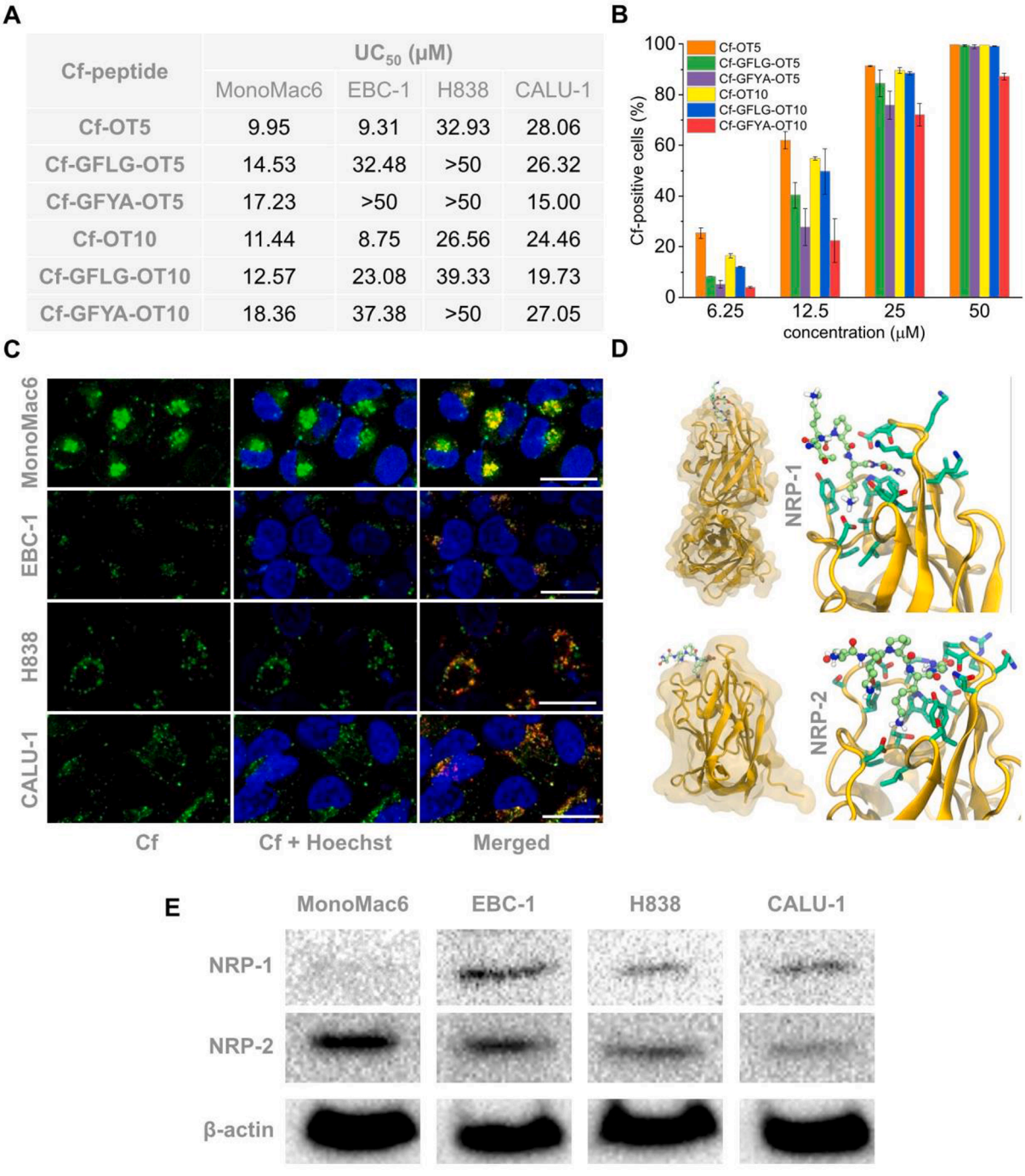

Fig. 3. The *in vitro* cellular uptake is characterized by UC_{50} values on MonoMac6, EBC-1, H838, and CALU-1 cells (**A**). *In vitro* cellular uptake on MonoMac6 cells (**B**). Intracellular localization of Cf-OT5 in MonoMac6, EBC-1, H838, and CALU-1 cells visualized by confocal microscopy (Panel **C**). Cells were treated for 3 h with Cf-peptides (25 μM, green). Lysosomes were stained by LysoTracker (red), nuclei were labeled by Hoechst (blue) (**C**). Potential binding of OT5 to NRP-1 and NRP 2 (**D**). NRP receptor content of whole-cell lysate of MonoMac6, EBC-1, H838, and CALU-1 cell cultures detected by Western blot. As a loading control, β-actin was used (**E**). (For interpretation of the references to colour in this figure legend, the reader is referred to the web version of this article.)

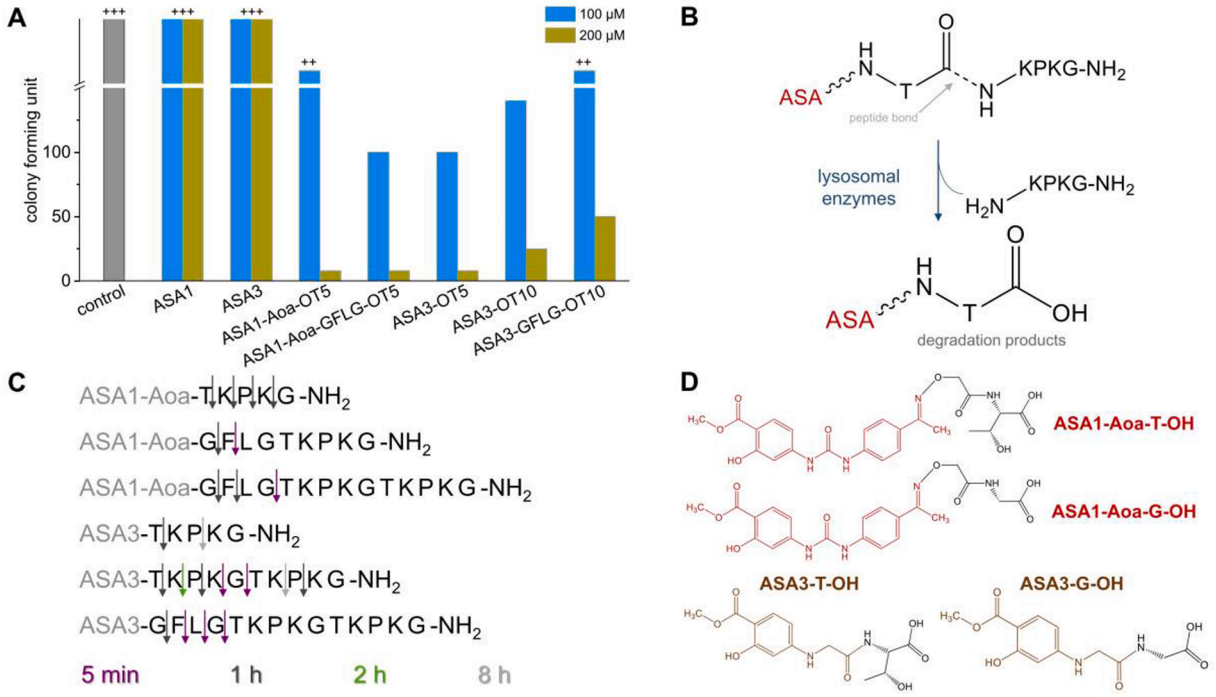

Fig. 4. Determination of efficacy on intracellular bacteria, the activity of the ASA derivatives, and their peptide conjugates on *Mtb* H_{37}Rv infected MonoMac6 cells (**A**). Lysosomal degradation profile of peptide conjugates (**B**, **C**). Lysosomes have an internal acidic pH (pH 4.5–5.0) and they contain various loads of hydrolytic enzymes, which play a crucial role in the intracellular drug release, lysosomal enzymes in action on peptide chain (**B**). Degradation of ASA-tuftsin conjugates in rat liver lysosomal homogenate (**C**). Structure of the detected main metabolites of the conjugates ASA1-Aoa-OT5, ASA1-Aoa-GFLG-OT5, ASA3-OT5, ASA3-OT10, and ASA3-GFLG-OT10 (**D**).

might be the consequence of an endosomal entrapment, while the diffuse intracellular distribution makes ASA-OT5 conjugates effective on intracellular *Mtb* (Fig. 4A).

Most of the Cf-peptides have higher uptake in the case of EBC-1 cells in comparison with H838 and CALU-1 cells. In the case of EBC-1 cells, Cf-OT5 has the highest (UC_{50} = 9.31 µM) and Cf-GFYA-OT5 (UC_{50} > 50 µM) has the lowest uptake (Fig. 3A). The UC_{50} values of Cf-OT5 and Cf-OT10 are at least three times lower compared to the linker-containing peptides, which means a significantly higher uptake. Based on CSLM imaging, the Cf-OT5 peptide has partial co-localization with the lysosomal staining (Fig. 3C).

The lowest uptake of Cf-peptides can be detected on H838 cells. Cf-O10 (UC_{50} = 26.56 µM) has the highest uptake, in the case of Cf-GFLG-OT5, Cf-GFYA-OT5, and Cf-GFYA-OT10 the UC_{50} values are higher than 50 µM. Cf-OT5 and Cf-OT10 have higher uptake compared to linker-containing peptides (Fig. 3A). Cf-OT5 mainly co-localizes with the lysosomal staining based on CLSM studies (Fig. 3C).

The effect of fixation was also investigated during CLSM studies. *In vitro* intracellular localization of Cf-OT5 was determined on living EBC-1 and H838 and fixed CALU-1 cells. The treating and staining conditions were standardized. According to our data, fixation has no effect in these cases on intracellular localization (Fig. 3C).

Interestingly, different tendencies can be observed on CALU-1 cells. Cf-GFYA-OT5 has the highest (UC_{50} = 15.00 µM) and Cf-OT5 has the lowest uptake (UC_{50} = 28.06 µM). In the case of CALU-1 cells, UC_{50} values were similar, smaller differences between the peptides were observed (Fig. 3A). Based on CLSM imaging, Cf-OT5 peptide has partial co-localization with the lysosomal staining (Fig. 3C). CLSM images of CALU-1 cells treated with Cf-peptides (25 µM, 3 h) are presented in SF106 and SF107.

In vitro cellular uptake of Cf-peptides was also determined on LCLC-103H cells. The concentration-dependent ratio of Cf-positive cells and fluorescence intensities are presented in the Supplementary Material (SF101-102). Based on CLSM studies, Cf-OT5 is co-localized mainly with the lysosomal staining in the case of LCLC-103H cells as presented in SF108.

In vitro cellular uptake and intracellular localization of selected compounds (Cf-OT5, Cf-GFLG-OT5, Cf-OT10) was determined on bone-marrow-derived cells (BMM*Φ*). The uptake of these compounds on BMM*Φ* cells is also concentration-dependent. Cf-OT10 has the highest uptake, followed by Cf-OT5 and Cf-GFLG-OT5 at all concentrations (SF103). Based on CLSM studies CF-OT10 mostly co-localizes, Cf-OT5, and Cf-GFLG-OT5 have partial co-localization with the lysosomal staining. CLSM images are presented in SF109.

2.10. Determination of neuropilin receptor occurrence by Western blot analysis

NRPs are a potential target on alveolar macrophages [52] infected with *Mtb*. Tuftsin-like peptide sequences are recognized by NRP receptors. NRP-1 and NRP-2 differ in their substrate preference; according to von Wronski *et al.* [56], tuftsin derivatives bind to NRP-1 with higher affinity than to NRP-2.

Based on visual molecular dynamics, OT5 (TKPKG) delivery peptide is capable of binding to the b1 domain of both NRP-1 and NRP-2 receptors (Fig. 3D). Thus, NRP receptors can serve as an entry for tuftsin delivery peptides *via* receptor-mediated endocytosis. As NRP-1 and NRP-2 are present in different host cells, targeting these receptors with tuftsin peptides is a promising strategy against intracellular *Mtb*.

The occurrence of NRP-1 and NRP-2 receptors on different cell cultures as host cell candidates was determined. MonoMac6 macrophages, and lung-originated EBC-1, H838, CALU-1, A549, and LCLC-103H cells were selected for lysis. We have established and optimized the Western blot process to detect NRP-1 and NRP-2 receptors from the whole cell lysates. Indirect detection of the receptors was used with anti-NRP-1 and anti-NRP-2 first antibodies, and anti-mouse-horseradish peroxidase

(HRP) secondary antibody. For experimental details and workflow see section *4.11.* and SF110A. To normalize protein levels of different cells, as a loading control, β-actin was used. In all cases, similar signals can be detected (Fig. 3E). Based on the loading control, the NRP-1 and NRP-2 receptor content of the cells can be compared.

Both NRP-1 and NRP-2 receptors are present in all cells (Fig. 3E). On MonoMac6 cells, NRP-1 is slightly observed. NRP-2 was detected with a high density, meaning high NRP-2 content of MonoMac6 cells. In the case of EBC-1 cells, both NRP-1 and NRP-2 were detected with high density. On H838 cells, higher NRP-2 content is observed compared to NRP-1. Oppositely, on CALU-1 cells higher NRP-1 receptor level is presented compared to NRP-2 (Fig. 3E). NRP-2 receptor was also detected on A549 and LCLC-103H as presented in the Supplementary Material SF110B.

2.11. Determination of efficacy against intracellular bacteria

As *Mtb* is an intracellular pathogen, it is indispensable to determine compounds' intracellular activity. As an infected macrophage model, sources of the monocytes are described in the literature, peripheral blood mononuclear cells (PBMC), and monoblastic/promyelocytic cells lines such as U937, THP-1, and HL-60, respectively. Cell lines can be expanded to reach vast numbers of cells and are reproducible. Since U937, THP-1, and HL-60 cell lines are not fully differentiated, they must be induced to develop phagocytic properties. MonoMac6 was established as a cell line, which appears to have phenotypic and functional characteristics of mature blood monocytes. MonoMac6 cells are phagocytic and express the CR3 receptor, which is important for the entry of *Mtb* bacteria [88,89]. Successful attempts have been shown that an infected MonoMac6 cell line is an appropriate model to determine *in vitro* activity of drug candidates against intracellular pathogens, for example, *Mtb*, *Legionella pneumophila*, and *Brucella abortus* [90–94]. In our previous studies, we have employed the *Mtb* infected MonoMac6 cells to determine the intracellular killing efficacy of different compounds, peptide conjugates, and nanoparticles [33,34,36,38,64,95,96]. In this work, the inhibition of intracellular bacteria was determined on MonoMac6 cells infected with *Mtb* H_{37}Rv.

After two treatments, free compounds did not have an intracellular effect in comparison with untreated control. Peptide conjugates inhibited the growth of intracellular bacteria, in a concentration-dependent manner (Fig. 4A). This intracellular efficacy of the conjugates can be explained by their enhanced cellular uptake in comparison with the free compounds.

For the efficient intracellular effect of conjugates, it is crucial to enhance not only the cellular uptake of free compounds but also to determine the rate of drug release. As tuftsin delivery peptides are mainly located in the lysosomal compartments, it is necessary to investigate lysosomal degradation patterns of conjugates and to identify metabolites containing active compounds (Fig. 4B).

The efficacy of the ASA-conjugates is related to their degradation and the intracellular drug release from the conjugates in the host cells. The degradation pattern of the conjugates in rat liver lysosomal homogenate was determined. For the identification of the products, a high-resolution HPLC-MS instrument was used. Mostly, no degradation of the amide or oxime bond between the compound and the peptides was detected (Fig. 4C). The smallest metabolites containing active compounds were the compounds and the first *N*-terminal amino acids (ASA1-Aoa-G-OH, ASA1-Aoa-T-OH, ASA2-Aoa-G-OH, ASA2-Aoa-T-OH, ASA3-G-OH, and ASA3-T-OH, Fig. 4D). The enzyme cleavable linker (GFLG, GFYA) containing peptide conjugates are digested faster and to a greater extent in comparison with the OT5 and OT10 conjugates. Generally, the GFYA linker is digested faster than the GFLG linker. Conjugates without enzyme-labile linkers have a similar degradation pattern, however, OT10 derivatives first degrade to OT5 peptides, thus, their degradation is overall slightly slower than in the case of OT5 conjugates.

The possible degradation ways of ASA-peptide conjugates from the synthetic point of view are presented in the Supplementary Material (SF111-113). Summary of the conjugates' degradation pattern is presented in the Supplementary Material (SF114). Base peak chromatograms and characterization of the detected metabolites are detailed for the conjugates in the Supplementary Material (SF115-132).

2.12. Determination of the penetration ability of Cf-OT5 on Transwell inserts

We have studied the penetration ability of the Cf-OT5 peptide on Transwell inserts using co-cultured, submerged, and non-contact monolayers as simple *in vitro* alveolar and bronchial barrier models. H838 or CALU-1 cells were seeded on the membrane of the apical chambers (Fig. 5A), and EBC-1 cells were used as detector monolayers on the basolateral surfaces (Fig. 5A, B).

Before the treatments, the confluency of the H838 and CALU-1 monolayer was monitored with CMFDA (Fig. 5C) and imaged *in situ*. Based on CMFDA staining, confluent monolayers were formed from both H838 (Fig. 5C) and CALU-1 cells (data not shown). The confluency and the occurrence of adherens junctions within the monolayer were also checked by β-catenin immunolabeling. β-catenin plays a role in the cell–cell adhesion and adherens junctions. β-Catenin associates with the cytoplasmic domain of the cadherin family adhesion receptors, anchoring them to the actin cytoskeleton and thus acting as a structural protein. Based on the enlarged representative microscopic images, adherens junctions can be detected between the H838 cells (Fig. 5D).

The penetration ability of Cf-OT5 was determined using CLSM image analysis. The penetration process was quantified by flow cytometry. In both cases, the intracellular fluorescence signal of the EBC-1 cells on the basolateral compartment was compared.

As the confluent monolayers were formed (usually after 5–6 days after seeding), Cf-OT5 were added to the apical chamber at 12.5, 25, and 50 μM concentration for 45 min or 3 h (Fig. 5A). As control experiments, treatments without TW were also carried out (Fig. 5B) (for experimental setup see SF133).

The penetration rates of peptide Cf-OT5 were quantified by flow cytometry (Fig. 5). Based on flow cytometry data, as expected the cellular uptake of Cf-OT5 on EBC-1 detector cells was higher without the inserts. The penetration across the Transwell inserts is time- and concentration-dependent in the case of H838 (Fig. 5E) and CALU-1 (Fig. 5F) monolayers, based on the mean fluorescent intensities.

The highest cellular uptake on EBC-1 detector cells was detected without Transwell inserts at 50 μM for 3 h, and the lowest was with Transwell inserts at 12.5 μM for 45 min. Interestingly, differences between the two types of interfaces containing H838 and CALU-1 were demonstrated. In the case of the H838 barrier, a higher penetration rate was detected towards EBC-1 cells. The percentage of Cf-positive cells also confirms these observations as presented in SF147. These results are in good agreement with the analysis of CLSM images.

EBC-1 cells on cover glass were stained and fixed before confocal microscopic analysis (Fig. 6A). According to confocal images (Fig. 6B, E, H, K), Cf-OT5 was able to cross the H838 monolayer and it was internalized into EBC-1 cells. For analysis of the visible differences between the CLSM images captured after treatments, NIH ImageJ software's Plot Profile application was used. Lines were drawn with a strictly similar orientation, starting from the cell nucleus towards cytoplasm on grayscale images (Fig. 6C, F, I, L). The obtained gray values correspond to the intensity of a given pixel on a scale of 0 to 255.

Based on the gray value analysis remarkable differences were observed between the treatments with and without the inserts containing H838 cells (Fig. 6D, G and Fig. 6J, M).

The penetration ability of Cf-OT5 across the interfaces was time- and concentration-dependent. In case of treatment with 12.5 μM for 45 min with Transwell insert no penetration was detected (Fig. 6E, F, G), while at 50 μM for 3 h, significant penetration was markedly detectable on the confocal image and the grayscale curves (Fig. 6K, L, M). The differences

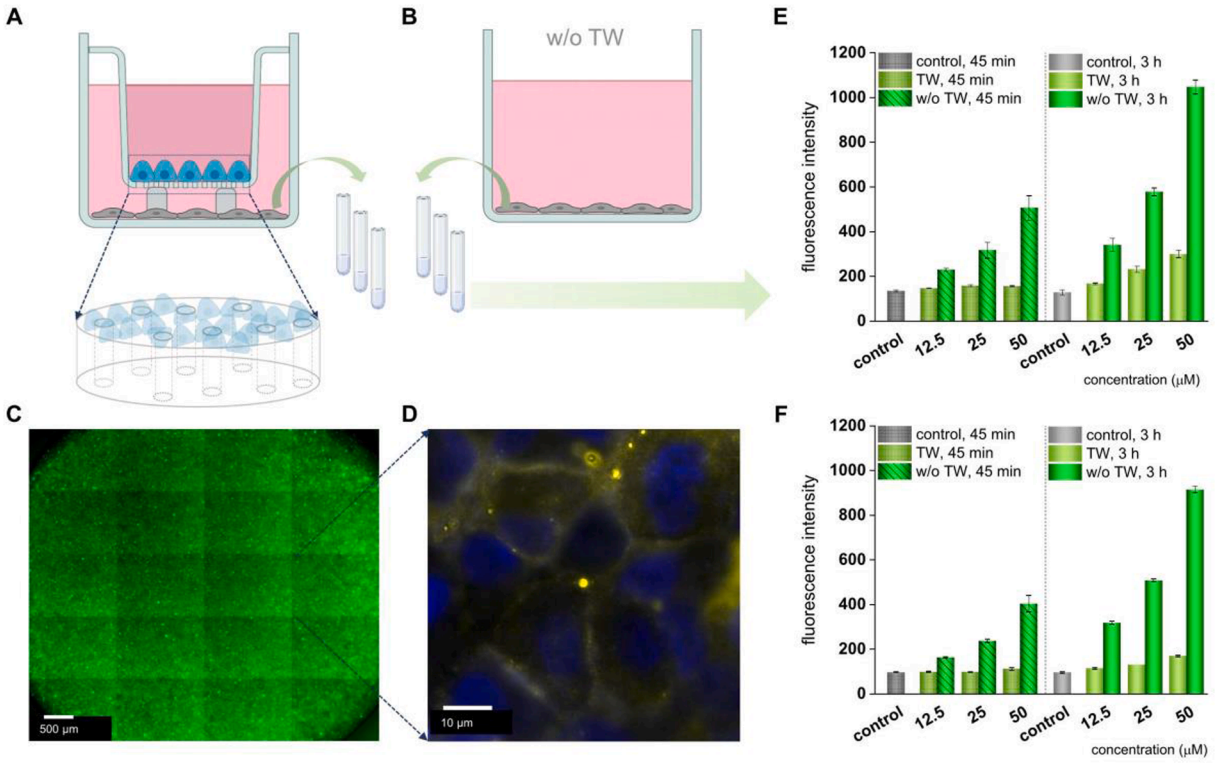

Fig. 5. The penetration ability of Cf-OT5 on Transwell inserts and the schematic representation of the experiment set up (**A, B**). H838 or CALU-1 cells were seeded on the apical side, EBC-1 cells were on the basolateral chamber's bottom (**A**, **B**). Enlarged features of the polycarbonate microporous membrane with H838 cells stained with CellTracker, and imaged *in situ* for multi-field mosaic image acquisition Scale bar represents 500 μm (**C**). A representative enlarged section, with β-catenin immunolabeling on an excised and mounted membrane stained with NucBlue (blue). Scale bar represents 10 μm (**D**). The penetration rates were monitored by flow cytometry through H838 (**E**) and CALU-1 (**F**) Cellular uptake of peptide Cf-OT5 was quantified by MFI values on EBC-1 detector cells (**E, F**). (For interpretation of the references to colour in this figure legend, the reader is referred to the web version of this article.)

were emphasized by the distribution of the families of curves in the diagrams on the right-hand side of Fig. 6. (Fig. 6D, G, J, M).

CLSM images corresponding to all treatments (at 12.5, 25, and 50 μM, 45 min or 3 h) and the gray value curves extracted from the outlined individual cells are presented in the Supplementary Material SF134-139 (H838 – EBC-1) and SF140-146 (CALU-1 – EBC-1), respectively.

2.13. The determination penetration ability of Cf-OT5 on tissue-mimicking EBC-1 spheroids

Next, we assessed the penetration ability of Cf-OT5 peptides on spheroids formed by EBC-1 cells. The schematic workflow using the agarose 3D Petri Dish with EBC-1 spheroids as a simple lung tissue-mimicking platform is presented in SF148.

Spheroids were treated within the agarose dishes with the Cf-peptide for 45 min and 3 h at 10 μM concentration (SF148C).

The EBC-1 spheroids had an average diameter of 400 and 450 nm (SF148D, E). Spheroids were fixed with 4% PFA, and then harvested and transferred from the agarose micro-wells into uncoated Ibidi chambers for CLSM imaging (SF148F, G, H). Line scan analysis of CLSM images was performed by NIH ImageJ software, using the Plot Profile application. Line scans were carried out using grayscale images, gray value corresponds to the intensity of a given pixel on a scale of 0 to 255. As spheroids are of various shapes and sizes, the diameter of the scanned area (horizontal axis distance) was normalized to 1 for better comparison. In the case of zonal scans, spheroids were selected in ImageJ, the selection was scaled to obtain zones, the scale factors are as follows: 1 for zone 1, 0.67 for zone 2, and 0.33 for zone 3. Intensity values were obtained by ImageJ and background corrected normalized fluorescence intensities (CNF) were calculated as described earlier [97].

To visualize the penetration profile of the Cf-OT5 we have carried out outline scan analysis extracted from the images (Fig. 7A). Spheroids were scanned in the z-direction with a step size of 10 μm (z1-z6) (Fig. 7B). The deepest z-section from the surface of a spheroid presented here is approx. 40 μm (z6) (Fig. 7C). To have comparable fluorescent intensity values among the zones, normalized gray value data were standardized as the proportion of the mean normalized intensity in the peripheries (0–100%).

Towards the center of the spheroids, the Cf-signal was gradually decreasing (Fig. 7D). Based on the presented results, we can conclude that Cf-OT5 has fair penetration ability on EBC-1 spheroids. Individual spheroids line scan and zonal scan analysis are presented in the Supplementary Material (SF149-151). Comparison of zonal scans is presented in SF152. The penetration ability to approx. 60 μm is presented in SF153.

3. Conclusion

Mycobacteria are uniquely adapted and equipped to survive within host cells [24–26], therefore the elimination of intracellular bacteria could be more efficient with directed delivery targeting host cell surface molecules and receptors (tuftsin, NRP, lectins, scavenger-, and mannosyl-receptors, etc.) [32,33,36,37,98–104].

In this study, a road map of an experimental approach to evaluate new antimycobacterial compounds and their tuftsin peptide conjugates was described. We intended to develop optimized conjugates (i) to target their infected host cells and release the antimycobacterial compounds in their active forms. We have synthesized new 4-aminosalicylic acid derivatives (ASA). As these derivatives were effective only against extracellular bacteria, the ASA derivatives were conjugated to host cell-specific peptide carriers. Tuftsin peptides were used as targeting moieties, as they are ligands for NRP receptors located on macrophages and

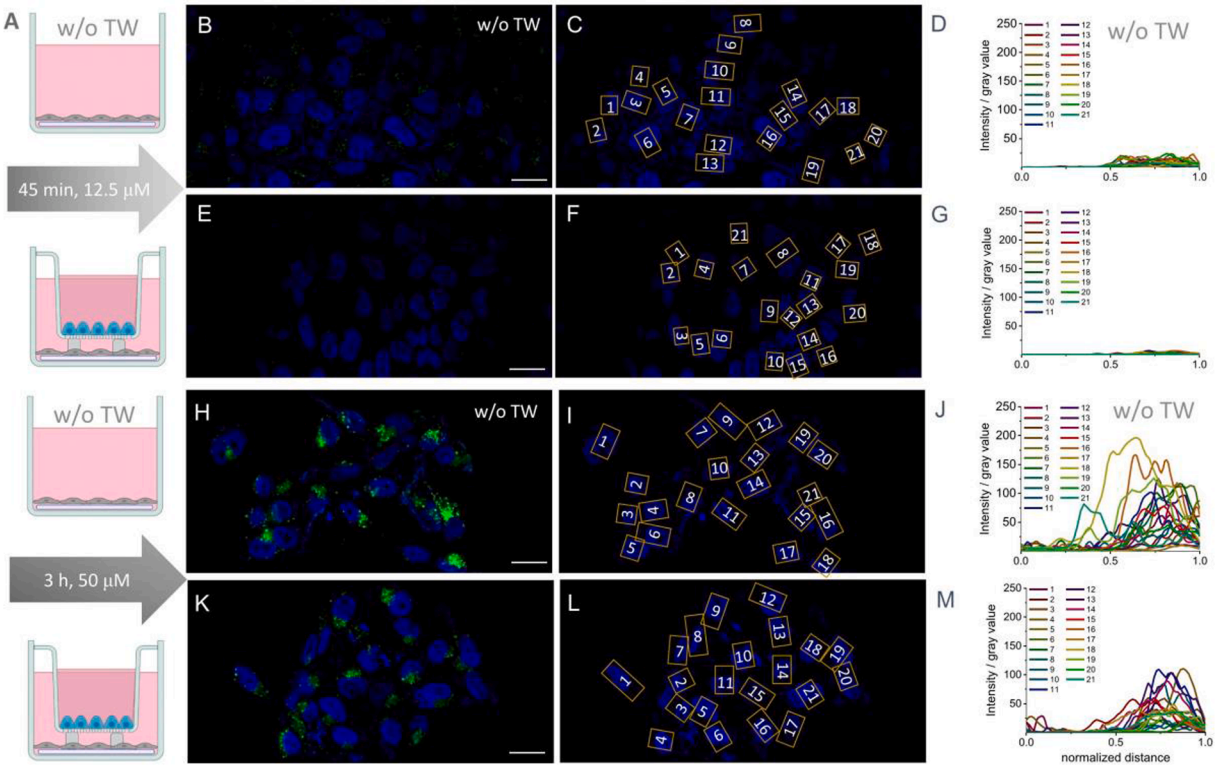

Fig. 6. The penetration process of peptide Cf-OT5 is followed by CLSM. H838 cells on the apical side, EBC-1 cells on the basolateral chamber's bottom on coverslips (Panel **A**). CLSM images of detector EBC-1 cells (Cf-OT5 (green): 12.5 μM, 45 min (**B**, **E**) and 50 μM, 3 h (**H**, **K**). Nuclei of EBC-1 were stained with Hoechst (blue). Scale bar represents 20 μm. Yellow rectangles indicate the area of (**C**, **F**, **I**, **L**) line scans. Lines were drawn starting from the cell nucleus towards the cytoplasm on grayscale images. The obtained gray values correspond to the intensity of a given pixel on a scale of 0 to 255. All line scan lengths were normalized to 1 yielding normalized diameter and the line scans were plotted (**D**, **G**, **J**, **M**). (For interpretation of the references to colour in this figure legend, the reader is referred to the web version of this article.)

lung tissue-related cells. Delivery tuftsin peptides were conjugated to the ASA compounds with or without enzyme-labile linker sequences (GFLG, GFYA). For the conjugation oxime (ASA1, ASA2) or amide (ASA3) bond was formed. All ASA derivatives and their conjugates have *in vitro* antimycobacterial effects against *Mtb* $H_{37}Rv$ bacteria and appropriate selectivity for monocyte MonoMac6 and lung-related cell cultures (EBC-1, H838, CALU-1, etc.) modeling the possible host cells. The membrane integrity of the host cells was also investigated by atomic force microscopy after treatments with free compounds and the conjugates. This method also demonstrated that the conjugation of the compounds decreased their cytotoxicity.

In vitro cellular uptake, intracellular localization, and penetration studies were obtained using fluorescent peptide derivatives. The tuftsin peptides have remarkable cellular uptake on monocytic and lung cell cultures. The intracellular localization studies proved the co-localization of the carriers with lysosomal dyes in all types of model cells. For intracellular efficacy, the release of the antimycobacterial compounds from the conjugates is also essential. As a proof-of-concept, the intracellular activity of the compounds was determined on *Mtb* $H_{37}Rv$ infected MonoMac6 cells. Free ASA derivatives were ineffective against intracellular bacteria, their peptide conjugates were able to inhibit (in a concentration-dependent manner) the intracellular bacteria. The lysosomal degradation pattern of the conjugates was determined employing rat liver lysosomal homogenates. In most cases, the smallest active metabolite was the first amino acid and the ASA compound.

The NRP receptor occurrence was determined using a newly established Western blot method. The significant presence of the NRP receptors was confirmed from the whole cell lysates. These data and the co-localization of the Cf-tuftsin peptides with the lysosomal compartment, imply receptor-mediated endocytosis as the main route of cellular internalization.

To demonstrate the *in vitro* penetration ability of the pentapeptide Cf-OT5 tuftsin, Transwell inserts were applied with bronchial or alveolar non-contact, co-cultured monolayers. This setup provided data on the trafficking pattern of the pentapeptide, mimicking lower respiratory tract tissue barriers. Furthermore, using 3D spheroid EBC-1 cultures for mimicking lung tissue *in vitro*, we have demonstrated that Cf-OT5 has fair penetration ability.

We have also demonstrated that Transwell insert and agarose-based spheroids could provide simple *in vitro* platforms for comparative penetration studies using confocal laser scanning microscopy and flow cytometry. For confocal images with line scan analysis, the quantification of differences is also a possible approach.

Taken together, with our experimental design and the applied assays, we characterized novel antimycobacterial compounds and their peptide conjugates. The employed sequence of the methods (*in vitro* MIC determination, selectivity, and localization studies to elucidate efficacy and specificity, infected host model, co-culture interface system on cell monolayers, and tissue-mimicking spheroids) was effective to find the most promising delivery peptides targeting intracellular *Mtb* with optimized features.

4. Experimental section

4.1. Materials

For the synthesis and chemical characterization of 4-aminosalicylic acid derivatives (ASA), reagents and solvents (4-aminosalicylic acid, methyl 4-aminosalicylate, 4-acetylphenyl isocyanate, ethyl acetate, methanol, toluene, triethylamine, sodium bicarbonate, dichloromethane, concentrated hydrochloric acid, glyoxylic acid monohydrate, sodium cyanoborohydride, glacial acetic acid, *n*-hexane, DMSO-d_6,

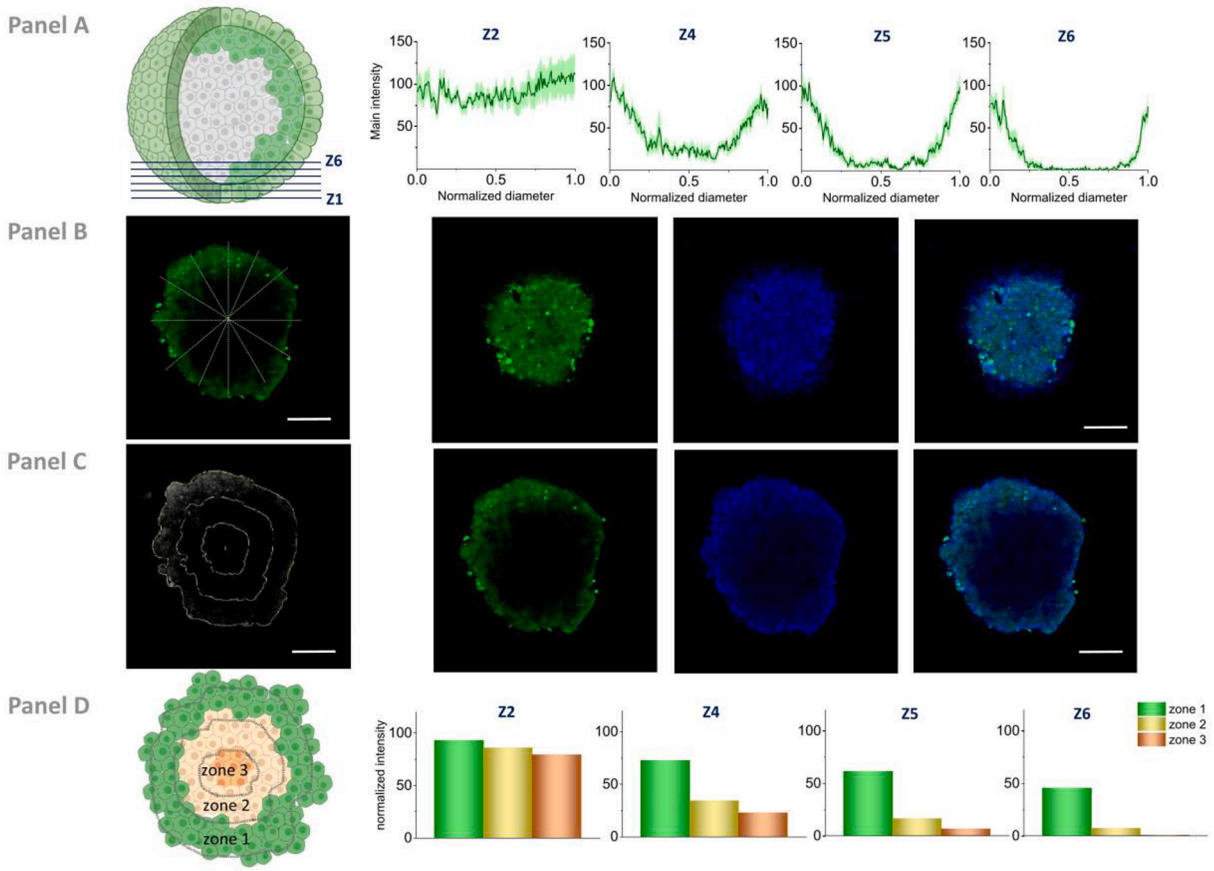

Fig. 7. Line scan and zonal scan analysis of CLSM images of EBC-1 spheroids following 3 h treatment with 25 μM peptide Cf-OT5. Line scans of spheroids at different (z2-z6) depth, mean intensities are gray values (0–255) averaged from 8 line scans, error stripes correspond to SEM (**Panel A**). Z-stack images were obtained with 10–15 μm intervals, the presented images are from the 10 μm (**z2, Panel B**) and 40 μm (**z6, Panel C**) depths; Cf-OT5 (green), nuclei were stained with Hoechst (blue). Scale bar represents 100 μm. Relative normalized intensity of spheroid zone 1, zone 2, and zone 3, data were extracted displaying the penetration ability of the peptide Cf-OT5; relative normalized intensities of spheroids were graphed at 10–40 μm (z2-z6) depths (**Panel D**). (For interpretation of the references to colour in this figure legend, the reader is referred to the web version of this article.)

tetramethylsilane) were purchased from Sigma-Aldrich (Darmstadt, Germany) or Penta Chemicals (Prague, Czech Republic).

For peptide synthesis amino acid derivatives, Boc-aminooxyacetic acid (Boc-Aoa-OH) and the Fmoc-Rink Amide MBHA resin were obtained from Iris Biotech GmBH (Marktredwitz, Germany). Reagents, such as, *N,N'*-diisopropylcarbodiimide (DIC), triisopropylsilane (TIS), 1-hydroxybenzotriazole (HOBt), 1,8-diazabicyclo[5.4.0]undec-7-ene (DBU), 1-methyl-2-pyrrolidone (NMP), piperidine, 5(6)-carboxyfluorescein (Cf), acetic anhydride, ethylene glycol monoethyl ether, citric acid, sodium acetate and disodium phosphate were purchased from Sigma-Aldrich (Budapest, Hungary). TFA, *N,N*-dimethylformamide (DMF), diethyl ether and acetonitrile were from VWR (VWR International, Debrecen, Hungary). *N,N*-diisopropylethylamine (DIEA) was from Fluka (Charlotte, NC, USA). Ninhydrin, isatin, acetic acid, dimethyl sulfoxide (DMSO) were from Reanal Laboratory Chemicals (Budapest, Hungary). Dichloromethane (DCM) (purity > 99.9%) was from Spectrum-3D Kft. (Debrecen, Hungary) and methanol was (purity > 99.9%) from Sigma-Aldrich.

For the *in vitro* assays RPMI-1640, DMEM medium, phosphate buffered saline (PBS) trypan blue, and L-glutamine were from Lonza (Basel, Switzerland). Pyruvate, trypsin, 3-(4,5-dimethylthiazol-2-yl)-2,5-diphenyltetrazolium bromide (MTT), recombinant murine macrophage colony-stimulating factor (rMu M−CSF), ethylenediaminetetraacetic acid (EDTA), paraformaldehyde (PFA), glutaraldehyde solution, Mowiol 4–88 and agarose were obtained from Sigma-Aldrich (Budapest, Hungary). Non-essential amino acids, fetal bovine serum (FBS) and Penicillin/Streptomycin (10,000 units penicillin and 10 mg streptomycin/mL) were from Gibco (Thermo Fisher Scientific, Waltham, MA, USA). HPMI buffer was prepared in our laboratory using components (glucose, $NaHCO_3$, NaCl, *N*-(2-hydroxyethyl)piperazine-*N'*-(2-ethanesulfonic acid - HEPES, KCl, $MgCl_2$, $CaCl_2$, $Na_2HPO_4 \times 2\ H_2O$) obtained from Sigma-Aldrich. Hoechst 33,342 (62249), LysoTracker Deep Red (L12492, for fixed cells), LysoTracker Red DND-99 (L7528, for living cells) and CellTracker Green Dye (CMFDA, C7025, 5-chloromethylfluorescein diacetate) were from Invitrogen Biotechnology (Thermo Fisher Scientific, Waltham, MA, USA). All buffers used during Western blot technique were made in-house using components obtained from VWR or AppliChem GmbH (Darmstadt, Germany). Acrylamide and *N,N'*-methylenebisacrylamide were obtained from Serva Electrophoresis GmbH (Heidelberg, Germany). Composition of buffers are presented in the Supplementary Material ST5. Anti-neuropilin-1 (sc-5307, produced in mouse), anti-neuropilin-2 (sc-13117, produced in mouse), anti-actin (sc-1616, produced in goat) antibodies and anti-goat-HRP secondary antibody (sc-2354, produced in mouse) were obtained from Santa Cruz Biotechnology (Dallas, TA, USA). Anti-mouse-horseradish peroxidase (HRP) secondary antibody (32430, produced in goat) and anti-rabbit Ig-Alexa555 (C2206, produced in donkey) were obtained from Invitrogen (Thermo Fisher Scientific, Waltham, MA, USA). Polyclonal anti-β-catenin antibody (A31572, produced in rabbit) was from Sigma (Budapest, Hungary).

4.2. Synthesis of 4-aminosalicylic acid (ASA) derivatives

The 4-aminosalicylic acid (ASA) derivatives were synthesized as

shown in Scheme 1. The reactions and the purity of the products were monitored by TLC using various mobile phases. Plates were coated with 0.2 mm Merck 60 F254 silica gel (Merck Millipore, Darmstadt, Germany) and were visualized by UV irradiation (254 nm). The melting points were determined on a Büchi Melting Point B-540 apparatus (BÜCHI, Flawil, Switzerland) using open capillaries and the reported values are uncorrected. Elemental analysis (C, H, N) was performed on an automatic microanalyzer CHNS-O CE instrument (FISONS EA 1110, Milano, Italy). Infrared spectra were recorded on a FT-IR spectrometer Nicolet 6700 using ATR-Ge method (ThermoFisher Scientific, Waltham, MA, USA) in the range of 650–4000 cm^{-1}. The NMR spectra were measured in DMSO-d_6 at ambient temperature using a Varian V NMR S500 instrument (500 MHz for ^{1}H and 126 MHz for ^{13}C; Varian Comp. Palo Alto, CA, USA). The chemical shifts (δ) are given in ppm with respect to tetramethylsilane used as an internal standard. The coupling constants (*J*) are reported in Hz. The details of the synthesis, chemical and structural characterization are described in the Supplementary Material.

4.3. Synthesis of tuftsin delivery peptides and peptide conjugates

Tuftsin delivery peptides were synthesized manually using standard Fmoc/^{t}Bu strategy as described in [36,62] (Scheme 3). Amide bond was formed on resin with the formation of *in situ* active ester. For the coupling 3 eq. of the free compound was dissolved in NMP, and DIC/HOBt coupling reagents were used (60 min) (Scheme 2A). Oxime bond was formed in liquid phase with the reaction of crude Aoa peptide derivatives and free compounds containing carbonyl group (ASA1, ASA2) [36,105,106] as shown in Scheme 2B. Crude products and reaction mixtures were purified using semi-preparative HPLC with reverse phase column. Details are described in the Supplementary Material.

To determine the homogeneity of the products and the stability of conjugates we applied analytical HPLC with reverse phase column. The products mass accuracy was determined using HR-MS. The details of the instruments, columns and the gradient are shown in the Supplementary Material.

Also, log*P* values were calculated using Chemicalize online platform. The basis of the calculation is detailed in the Supplementary Material.

4.4. Cell culturing

MonoMac6 human monocytes (Deutsche SammLung von Mikroorganismen und Zellkulturen, DSMZ no.: ACC 124) [88–90], EBC-1 lung squamous carcinoma (CVCL_2891) [107,108], H838 human lung adenocarcinoma (American Type Culture Collection, ATCC CRL-5844) [108], CALU-1 human lung epidermoid carcinoma (Sigma 93120818) [109,110], for the *in vitro* evaluation studies. For maintaining MonoMac6 cell cultures RPMI-1640 medium supplemented with 10% FBS, 2 mM L-glutamine and 160 μg/mL gentamicin (CM RPMI-1640) was used. In case of EBC-1, H838 and CALU-1 cell cultures DMEM supplemented with 10% FBS, 2 mM L-glutamine, 100 μg/mL Penicillin/Streptomycin, 1 mM Pyruvate and 1% non-essential amino acids (CM DMEM) were used. Cells were incubated at 37 °C, 5% CO_2 humidified atmosphere.

Murine bone marrow culture-derived macrophages (BMMΦ) were also used in our study. The culture of BMMΦ macrophages were prepared as described earlier [78,82–85]. We have differentiated BMMΦ cultures from frozen stocks of the isolated bone marrow cells (the isolation process and experiments were approved by the Hungarian Scientific Ethical Committee on Animal Experimentation (No: XIV-I-001/2149–4/2012). The log-phase growth of the BMMΦ was maintained by culturing in rMu M−CSF in RPMI 1640 medium supplemented with 0.16 mg/mL gentamicin, 2 mM glutamine; 10% FBS, 10 mM HEPES and 10 ng/mL rMu M−CSF (recombinant murine macrophage colony-stimulating factor, Sigma M9170). Prior to the experiments, cells were washed three times with PBS. The macrophages were harvested with PBS (0.1 M, pH 7.4) containing 10 mM EDTA and seeded using the media with content above.

4.5. Determination of in vitro antimycobacterial effect

Mtb $H_{37}Rv$ (ATCC 27294) were grown in Sauton's liquid medium to exponential growth phase (approx. 3–4 weeks). The Sauton's medium was prepared in-house as described in [111] with the addition of 0.05% (w/v) Tween-80 to prevent bacterial aggregation (since *Mtb* $H_{37}Rv$ tends to form clumps). The bacterial suspension was homogenized by ball-milling using sterilized stainless steel grinding balls and after dilution, it was used for the inoculation of the test tubes.

Antimycobacterial activity of the ASA compounds and their peptide-conjugates was determined on *Mtb* $H_{37}Rv$ using conventional broth-dilution method in Sula semisynthetic medium (pH = 6.5) [112,113]. Dilution series of the compounds were prepared in DMSO and added to test tubes [32,36,77–80,114–118]. The bacterial suspension (1.5×10^4 CFU/mL) was added to the test tubes. The minimal inhibitory concentration (MIC, reported in μM, μg/mL) was determined after incubation at 37 °C for 28 days. MIC was the lowest concentration of a compound at which no visible growth of the bacteria occurred. The antimycobacterial effect of the tested compounds were confirmed using a colony forming unit (CFU) determination by sub-culturing 100 uL of the supernatant onto drug-free Löwenstein-Jensen solid medium (37 °C, 28 days), which is a selective medium specifically used for the culture and isolation of *Mtb* $H_{37}Rv$ [119,120]. Experiments were repeated at least two times. As reference compound isoniazid was used.

All experimental procedures with infectious *Mtb* were performed in a Biosafety Level 3 (BSL-3) laboratory at the National Public Health Center (Hungary), respecting the institutional containment level 3 laboratory management and biosecurity standards, based on applicable national and EU Directives.

4.6. Determination of in vitro cytostatic and cytotoxic effect

In vitro cytostatic – antiproliferative - effect of ASA derivatives, conjugates and Ac-peptides were determined on MonoMac6, EBC-1, H838 and CALU-1 cells using MTT assay. *In vitro* cytotoxic effects of selected conjugates (ASA1-Aoa-OT5, ASA1-Aoa-GFLG-OT5, ASA3-OT5, ASA3-OT10) were also determined with MTT assay.

For the MTT assay, cells were seeded during the exponential growth phase, one day prior to the experiment. In case of cytostasis 5×10^3 cells/100 μL/well, for cytotoxicity 1.5–2.0 $\times 10^4$ cells/ 100 μL/ well were seeded on a 96-well cell culture plate (Sarstedt, Germany) in CM. Cells were treated with the compounds dissolved in RPMI-1640 or DMEM incomplete medium (ICM) with 1% (v/v) DMSO in the concentration range 2.56×10^{-3} – 200 μM (Ac-peptides and conjugates) or 6.4×10^{-4} – 50 μM (ASA compounds). In case of cytotoxicity studies 3.2×10^{-3} – 250 μM concentration range was used. Cells were treated with the compounds for 20–24 h. As control ICM and ICM containing 1% (v/v) DMSO were used. In case of cytostasis studies, cells were washed with ICM three times, and in the last step, CM was added. After culturing the cells for 48–72 h, 45 μL sterile-filtered MTT (Millex 0.22 μm filter, Millipore, Cork, Ireland) was added (2 mg/mL in ICM) to the cells. In case of cytotoxicity, MTT was added to the cells immediately after washing. Mitochondrial enzymes reduce MTT to a formazan derivative (purple crystals) [121–123].

After 3.5 h incubation, plates were centrifuged (2000 rpm, 5 min), supernatant was removed, and formazan crystals were dissolved in DMSO. Absorbance was determined with an ELISA plate reader (Labsystems iEMS reader, Helsinki, Finland) at λ = 540 and 620 nm. A_{620} values were subtracted from A_{540} values, and cytostatic or cytotoxic activity was calculated with the formula: cytostasis/cytotoxicity% = $100 \times (1\text{-}A_{\text{treated cells}}/A_{\text{control cells}})$, where $A_{\text{treated cells}}$ and $A_{\text{control cells}}$ are the average absorbance of treated and control cells. The 50% inhibitory concentration (IC_{50}) values were determined from the dose–response curves. The curves were calculated with Microcal OriginPro (version:

2018) software.

4.7. Membrane integrity studies using atomic force microscopy

MonoMac6 and EBC-1 were seeded in CM to 24-well cell culture plates (Greiner Bio-One, Hungary), which contained cover glasses (thickness 1, Assistant, Karl Hecht GmbH & Co KG, Sondheim/Rhön, Germany) 24 h before the experiment (10^5 cell/ 1 mL/ well). Cells were treated with the conjugates (ASA1-Aoa-OT5, ASA2-Aoa-OT5 and ASA3-OT5) for 3 h at 250 μM (37 °C, 5% CO_2). Control cells were incubated with ICM. After the treatment, cells were washed two times with ICM and two times with PBS. Cells then were fixed with 4% glutaraldehyde (dissolved in PBS) for 20–24 h at 4 °C. After the fixation cells were washed two times with PBS and two times with distilled water.

Surface morphology of the fixed cells was investigated with AFM. High resolution imaging of the surfaces was performed with a Nanosurf Flex-Axiom AFM system operating in dynamic mode utilizing soft-tapping cantilevers (Tap150-G, BudgetSensors) with nominal force constant of 5 N/m. The apex area of the cells was selected for imaging with a scan area of 2 μm × 2 μm (512 × 512-pixel resolution), where the cellular curvature has the smallest distortion effect on the recorded height profiles.

4.8. Determination of in vitro cellular internalization

To determine *in vitro* cellular uptake of the Cf-peptides BD LSR II (BD Biosciences, San Jose, CA, USA) flow cytometer was used. *In vitro* cellular uptake of Cf-peptides was determined on MonoMac6, EBC-1, H838 and CALU-1 cells. Cells were seeded during the exponential growth phase one day prior to the experiment to 24-well cell culture plates (Greiner Bio-One) with a density 10^5 cells/ 1 mL/ well in CM. Dilution series were prepared in ICM with 1% DMSO (v/v) in the concentration range 6.25 – 50 μM. Cells were treated with the Cf-peptides for 3 h (in case of MonoMac6 cells 1.5 h treatment was also performed), and then they were washed once with ICM and once with HPMI buffer (9 mM glucose, 10 mM $NaHCO_3$, 119 mM NaCl, 9 mM HEPES, 5 mM KCl, 0.85 mM $MgCl_2$, 0.053 mM $CaCl_2$, 5 mM $Na_2HPO_4 \times 2\ H_2O$, pH 7.4) [124]. To remove the surface bound peptides and detach cells from the plate 100 μL trypsin was added to the cells for 2 min (MonoMac6), 12 min (EBC-1), 5 min (H838, CALU-1). Trypsin activity was stopped with 800 μL HPMI medium supplemented with 10% FBS (v/v). Cells were then transferred into FACS tubes (Sarstedt), centrifuged (5 min, 1000 rpm) and after removing the supernatant, 300 μL HPMI was added. Intracellular fluorescence intensity of cells was measured at $\lambda_{ex} = 488$ nm (Coherent Sapphire laser excitation, emission channel - LP 510, BP 530/30). Results were analyzed with FACSDiva software.

Cells were first gated on size and granularity (SSC vs FSC), then live cells were gated by using propidium iodide (PI), which dye can penetrate cell membranes of dying or dead cells. To identify the internalization of Cf-peptides, live cells were divided into FITC positive and FITC negative subpopulations. The cell viability was assessed using 10 μg/mL propidium iodide (PI) solution. The intracellular fluorescence intensity of the cells was measured on channel PE LP550 (emission at $\lambda = 550$ nm) and data were analyzed with FACSDiva 5.0 software. All measurements were performed in triplicates.

Trypan blue was also used to distinguish membrane-bound peptides from internalized ones by quenching the external fluorescence. Trypan blue is impermeable for living cells and quenches the extracellular green fluorescence, therefore, only the internal fluorescence can be detected. This quenching was performed by adding 10 μL of 0.04% trypan blue solution to the cells. Intracellular fluorescence intensity of cells was measured by flow cytometry before and after adding trypan blue.

4.9. In vitro intracellular localization using confocal laser scanning microscopy (CLSM)

MonoMac6 and CALU-1 cells were seeded in CM to 24-well cell culture plates (Greiner Bio-One), which contained cover glasses (Assistant) 24 h before the experiment (10^5 cells/ 1 mL/ well). Cells were treated with the Cf-peptides (concentration: 25 μM) for 3 h in ICM. Lysosomes were stained with LysoTracker Deep Red, nuclei were stained with Hoechst 33342, according to the manufacturer's suggestions. After every staining step, cells were washed three times with ICM. Before fixation, cells were washed two times with PBS. Cells were fixed with 4% PFA for 20 min at 37 °C. After fixation cells were washed three times with PBS and two times with distilled water. Cover glasses were mounted to microscopy slides (VWR) by Mowiol 4–88 mounting medium.

For living cells' uptake analysis EBC-1 and H838 cells were seeded to ibiTreat 15 μ-slide 8 well (ibidi GmbH, Grafelfing, Germany) 24 h before the experiment (3×10^4 cells/ chamber/300 μL CM). Cells were treated with Cf-OT5 as described above (concentration: 25 μM) for 3 h in ICM. Lysosomes were stained with LysoTracker Red DND-99, nuclei were stained with Hoechst 33342.

Confocal microscopy studies were performed on a Zeiss LSM 710 system (Carl Zeiss Microscopy GmbH, Jena, Germany) with a 40 × oil objective with the parameters: Cf-peptides $\lambda_{ex} = 488$ nm, $\lambda_{em} = 541$ nm, nuclei $\lambda_{ex} = 405$ nm, $\lambda_{em} = 467$ nm (Hoechst 33342), lysosomes $\lambda_{ex} = 633$ nm, $\lambda_{em} = 720$ nm (LysoTracker Deep Red) or $\lambda_{ex} = 577$ nm, $\lambda_{em} = 590$ nm (LysoTracker Red DND-99) were used. Zeiss ZEN lite software (Carl Zeiss Microscopy GmbH) was used for image processing.

4.10. Determination of compound efficacy against intracellular bacteria

To assess of intracellular inhibition activity of the ASA compounds and their peptide conjugates on the previously published method [90,91] was developed (first described by Horváti et al. [33]) and have been used since then in our research [34,36,38,64,95,96]. Briefly, MonoMac6 monocytes (2×10^5 cells/1 mL medium/well) were cultured with RPMI-1640 medium containing 10% FBS. Adherent cells were infected with *Mtb* $H_{37}Rv$ at a multiplicity of infection (MOI) of 10 for 4 h. Extracellular bacteria were removed, and the culture was washed three times with RPMI-1640 ICM. The infected monolayer was incubated for 1 day before the treatment. Infected cells were then treated with compounds at 100 and 200 μM final concentration. After 3 days the treatment was repeated with freshly prepared solution of compounds for an additional 3 days. Untreated cells were considered as negative control. After washing steps - in order to remove the compounds - infected cells were lysed with 2.5% sodium dodecyl sulfate solution. The CFU of *Mtb* was enumerated on Löwenstein-Jensen solid media after 4 weeks of incubation.

All experimental procedures with infectious *Mtb* were performed in a Biosafety Level 3 (BSL-3) laboratory at the National Public Health Center (Hungary), respecting the institutional containment level 3 laboratory management and biosecurity standards, based on applicable national and EU Directives.

4.11. Determination of neuropilin receptor occurrence by Western blot analysis

MonoMac6, EBC-1, H838 and CALU-1 cells were analyzed for their occurrence of NRP receptors using Western blot detection. All buffers were made in-house; compositions are summarized in the Supplementary Material ST5. Process of Western blot technique is presented in Supplementary Material SF109B. Cells were harvested with trypsinization, and after washing with PBS, cells were lysed for 30 min at 4 °C in lysis buffer. After the lysis, samples were centrifuged with 13500 rpm for 30 min at 4 °C. Supernatants were collected and stored at −80 °C. Protein concentration of samples was determined using Qubit Protein

Assay Kit (Thermo Fisher Scientific) according to the manufacturer's instructions. Equal amount of proteins was run on 10% Tris-tricine gel [125]. Proteins were blotted in a Towbin buffer (pH ~ 8.3) with 350 mA for 45 min to polyvinylidene fluoride (PVDF) membrane with a Bio-Rad Wet Blotting System (Bio-Rad Hungary, Budapest, Hungary). For the blocking 4% milk powder in TBS-Tween buffer (pH ~ 7.4) was used for 1 h. NRPs were detected by anti-NRP-1 antibody (1:75) and anti-NRP-2 antibody (1:75) and an anti-mouse-horseradish peroxidase (HRP) secondary antibody (1:500). β-actin was used as loading control and was detected by anti-actin antibody (1:2000) and an anti-goat-HRP secondary antibody (1:2500). After the addition of enhanced chemiluminescence (ECL) substrate (SuperSignal West Pico PLUS Chemiluminescent Substrate, Thermo Fisher Scientific), the chemiluminescent signal was detected by ChemiDoc XRS + Detection System (Bio-Rad Hungary).

4.12. Visual molecular dynamics using PDB structures

Illustrations showing the potential binding of OT5 to NRP-1 and NRP-2 were created using visual molecular dynamics (VMD) v1.9.31 based on protein data bank (PDB) entries 2ORZ and 5DN2, respectively. The bound peptides of the respective NRPs in the initial PDBs were replaced by OT5 using an "in-house-developed" python program. The program performs an angle and dihedral angle fitting on the target (OT5) peptide based on a pre-given correspondence list of target and reference residues followed by an RMSD fitting of the target to the reference peptide. Thus, the method allows quick fitting of two different peptides based on a subset of potentially dissimilar residues.

4.13. Determination of lysosomal digestion pattern of the conjugates

Rat liver lysosomal homogenate (protein content: 16.6 μg/μL) was prepared as described in [126]. Conjugates were dissolved in 0.2 M sodium acetate buffer (pH = 5.0, 16.4 mg/mL) to a concentration of 50 pmol/μL. Rat liver lysosomal homogenate was diluted in 0.2 M sodium acetate buffer to a concentration 4.15 μg/μL. This diluted homogenate was added to the conjugates in a ratio 1:1 (w/w). As controls, conjugates dissolved in sodium acetate buffer and lysosomal homogenates without conjugates were used. Reaction mixtures were incubated at 37 °C with shaking (600 rpm). Reaction was terminated with 2 μL acetic acid at 5 min, 1, 2, 4, 8 and 24 h. Control samples were taken at 5 min and 24 h. Samples were stored at −80 °C until measurement [36,126].

For the HPLC-MS measurement samples were diluted in distilled water and were stored at 4 °C. Degradation products were identified with Thermo Scientific Ultimate 3000 UHPLC system - Q Exactive Focus Hybrid Quadrupole-Orbitrap Mass Spectrometer using on-line UHPLC coupling. UHPLC separation was performed on a Supelco Ascentis C_{18} (2.1 × 150 mm, 3 μm) column. Eluent A was distilled water with 0.1% (v/v) formic acid, eluent B was acetonitrile: water = 80:20 (v/v) with 0.1% formic acid. Flow rate: 0.2 mL/min, gradient: 0–2 min 2% B, 2–26 min 2–90% B, 26–27 min 90–100% B, 27–28 min 100% B, 28–28.5 min 2% B, 28.5–30 min 2% B. Target mass range was 150–1600 *m/z* in a positive mode with 3.0 μL/min flow rate. Results were evaluated using Thermo Scientific Xcalibur Software.

4.14. Determination of the penetration ability of Cf-OT5 on Transwell inserts

In preliminary experiments different Transwell inserts (TW) were tested including comparison of brand, insert pore sizes and seeding procedures (as described earlier [97]). For cell culturing and maintenance of H838, CALU-1 and EBC-1 see section (4.4 Cell culturing).

24-well plates with Transwell inserts (Nunc, Sigma) of 0.4 μm pore size were used for barrier seeding. Before use, the TW inserts with polycarbonate microporous membrane were incubated with ICM (growth area 0.412 cm^2). On day one, 300 μL of H838 or CALU-1 suspension in CM DMEM (8.5 × 10^4 cells) was pipetted onto the surface of the Transwell apical chamber and 500 μL DMEM ICM was added to the basolateral side. In order to avoid non-attached cells, after incubation at 37 °C for 5–6 h, the apical medium was removed and replaced with fresh CM DMEM. On day three, medium was changed and H838 or CALU-1 cells were grown up to confluence (which was checked prior to and after the experiments).

The confluence was monitored with CMFDA. CMFDA was dissolved in ICM DMEM medium to reach 5 μM concentration. After 15–45 min of incubation time, the cells were washed with DMEM ICM. After development of stable green fluorescence, cells were imaged *in situ*. Image acquisition was performed using a Zeiss Axio Observer Z1 inverted epifluorescent microscope with 10 × Plan Neofluar or 40 × EC Plan-Neofluar objectives. The microscope was equipped with a Zeiss AxioCam MRm CCD camera and a Marzhauser SCAN-IM powered stage. For multi-field mosaic image acquisition, stage positioning and focusing were controlled by Zeiss Axiovision 4.8 software. Images were processed using National Institute of Health (NIH) ImageJ software.

The confluency of the monolayers on Transwell's polycarbonate microporous membrane was also checked by β-catenin immunolabeling. The process was performed as described earlier [127]. β-Catenin plays a role in the cell–cell adhesion, in adherens junctions, β-catenin associates with the cytoplasmic domain of the cadherin family adhesion receptors, anchoring them to the actin cytoskeleton and thus acting as structural protein [128]. Briefly, cells were washed with 4% PFA in PBS then permeabilized (0.1% Triton X-100 in PBS). Non-specific binding sites were blocked with 1% bovine serum albumin (BSA) in PBS. Beta-catenin was labeled using rabbit polyclonal anti-beta-catenin antibody (Sigma - C2206) as primary antibody in 1:100 dilution at 4 °C overnight and anti-rabbit Ig-Alexa555 (Invitrogen - A31572) as secondary antibody in 1:200 dilution for 3 h at room temperature. Finally, Transwell membranes with the immunolabeled cells were excised from the Transwell unit and mounted on microscopic slides (Thermo Scientific) in Prolong mounting medium with NucBlue (Hoechst 33342) counterstain (Thermo Fisher) and imaged subsequently.

On day five or six, before the Cf-peptide treatment, medium was changed on Transwell monolayers. Cf-peptide was added to the apical side at 12.5, 25 and 50 μM concentrations and the system was incubated for 45 min or 3 h (37 °C, 5% CO_2). The Transwell chamber was removed after incubation. As detector culture on the basolateral side of the chamber, EBC-1 cells' uptake was studied using flow cytometry (BD LSR II).

EBC-1 cells were treated without the presence of the Transwell inserts as controls (on day four prior to treatment, EBC-1 cells (10^5 cells/well in CM DMEM) were seeded on 24-well plates).

On day four or five prior to Transwell treatment, EBC-1 cells (10^5 cells/well in CM DMEM) were seeded on cover glasses (Assistant, see: 4.9.) inserted in the basolateral chambers of 24-well plates. Cf-OT5 was added to the H838 or CALU-1 Transwell monolayers containing apical side at 12.5, 25 and 50 μM concentrations and the cells were incubated for 45 min and 3 h (37 °C, 5% CO_2). The Transwell chamber was removed after incubation. Cell nuclei of EBC-1 cells form the basolateral chamber were stained with Hoechst 33342, according to the manufacturer's suggestions. EBC-1 cells were fixed with 4% PFA and mounted on microscopy slides with Mowiol 4–88 as described in section *4.9. In vitro intracellular localization using confocal laser scanning microscopy (CLSM)*. Fixed EBC-1 cells were studied using confocal microscopy (Zeiss LSM 710). EBC-1 cells were treated without the presence of the TW inserts as controls. The same conditions were used for detection of Cf-signal and Hoechst 33,342 as described in section *4.9*. Laser intensity values were identical. ZEN 3.0 blue lite software was used for image processing. This was performed by NIH ImageJ software using the Plot Profile application. On grayscale images outlines were drawn with similar orientation, starting from the cell nucleus towards the cytoplasm. The obtained gray values correspond to the intensity of a given pixel on a scale of 0 to 255. All line scan lengths were normalized to 1 yielding normalized diameter

and the line scans were plotted using software OriginPro 2018.

4.15. Determination of the penetration ability of Cf-OT5 on tissue-mimicking EBC-1 spheroids

In this study we have employed a modified method based on [97]. Briefly, micro-molds for casting 3D Petri Dishes (MicroTissues, Sigma, 9 × 9 array) were filled with molten agarose (2%, w/v in PBS). The gelled agarose dishes were equilibrated with DMEM ICM (2 mL / 2 h, 37 °C). Cells were seeded using 20 μL cell suspension (2.2×10^4 cell /μL in DMEM CM). Prior to seeding process nuclei were stained with Hoechst 33,342 solution (0.2 μM) for 30 min. Based on our previous work with spheroids [97] the nuclear stain could not successfully penetrate into deeper layers of the spheroids (mostly localized at the spheroid surface) and towards the center of the spheroids the Hoechst 33,342 signal was gradually decreasing. Stained seeded cells were incubated in 2 mL DMEM CM for 48 h while cell-to-cell adhesion drives the aggregation and formation of spheroids.

To monitor the condition of the spheroids, bright-field images were captured using an Olympus CX41 microscope. After 48 h of incubation, spheroids were washed two times with fresh ICM DMEM and they were treated in the micro-wells with the Cf-OT5 peptide (25 μM / 2 mL ICM DMEM for 3 h). After the treatment, spheroids were washed two times with ICM DMEM and three times with PBS. Spheroids were fixed with 4% PFA for 15 min (37 °C). Spheroids were washed three times with PBS and then harvested and transferred from the agarose micro-wells into μ-Slide 8 well uncoated Ibidi chambers for imaging (Zeiss LSM 710; 10 × dry objective (10×/0.45 M27)). The same excitation and emission wavelengths were used as for the 2D CLSM imaging. Z-stack images were obtained by scanning the spheroids from the bottom of the spheroid with 11 μm distance between each scanning plane. Images were processed with ZEN 3.0 blue lite software. Line scan analysis was performed by NIH ImageJ software, two spheroids were analyzed (8 scans per spheroid, n = 16 in total). Line scans were carried out using grayscale images, gray value corresponds to the intensity of a given pixel on a scale of 0 to 255. As spheroids are of various shapes and sizes, the diameter of the scanned area (horizontal axis distance) was normalized to 1 for better comparison. To average the intensity values from line scans of spheroid sections of slightly different size and shape all line scan lengths were normalized to 1 yielding normalized diameter. Calculation of average and SEM of multiple curves was carried out using software OriginPro 2018.

In case of zonal scans, spheroids were selected in ImageJ, selection were scaled to obtain zones, the scale factors are as follows: 1 for zone 1, 0.67 for zone 2 and 0.33 for zone 3. Intensity values were obtained by ImageJ and background corrected normalized fluorescence intensities (CNF) were calculated as follows: CNF = ((ID – (A × MFB))/A, where ID is integrated density, A is area, MFB is mean fluorescence of background based on Baranyai *et* al. [97].

Author contributions

Conceptualization: SB. Design, synthesis and chemical characterization of the ASA compounds, delivery peptides and conjugates: MK, VP, JV, SB, LBH, ZB. Design, preparation of the *in vitro* monolayer based methods, analysis - interpretation of the results: SB, LBH. Work with extracellular *Mtb* cultures: SB, LBH. *Mtb* infected MonoMac6 assays: SB, Design, preparation, analysis of the spheroids: SB, LBH, BBK, ELM. Design of the Transwell experiments: SB, Preparation and analysis of the Transwell experiments' data: SB, LBH, EM, *Ex vivo* membrane integrity studies and analysis: GG, Western blots: LBH, BBK, Confocal microscopy image acquisition and analysis: ÁB, LBH, SB. Molecular imaging: GK, Writing the manuscript: LBH, SB. The manuscript was written through contributions of all authors. All authors have given approval to the final version of the manuscript.

Declaration of Competing Interest

The authors declare that they have no known competing financial interests or personal relationships that could have appeared to influence the work reported in this paper.

Acknowledgments

This work was completed in the ELTE Thematic Excellence Programme 2020 supported by National Research, Development and Innovation Office - TKP2020-IKA-05. This work was supported by the National Research, Development and Innovation Office, Hungary (grants: VEKOP-2.3.3-15-2017-00020). This work was supported by the Czech Science Foundation [grant number 20-19638Y]; the EFSA-CDN [grant No. CZ.02.1.01/0.0/0.0/16_019/0000841] co-funded by ERDF and SVV 260 547.

SB, LBH ELM thank for the support of grant EFOP-1.8.0-VEKOP-17-2017-00001. We are grateful for the ELTE Thematic Excellence Programme (Szint +) and the 2018-1.2.1-NKP-2018-00005 project (under the 2018-1.2.1-NKP funding scheme) provided by the Hungarian Ministry for Innovation and Technology and for the National Research, Development and Innovation Office, Hungary.

The authors thank Bálint Szeder (Research Centre for Natural Sciences) for assistance in confocal microscopy and Eleonóra Szabó, Sándor Dávid (National Korányi Institute of Pulmonology) and Kata Horváti (ELKH-ELTE Research Group of Peptide Chemistry, Eötvös Loránd Research Network, Eötvös Loránd University) for the assistance in mycobacterial work. GG thanks for the János Bolyai Research Scholarship of the Hungarian Academy of Sciences.

Figs. 5-7 were created partially with BioRender.com. Marvin was used for drawing, displaying and characterizing chemical structures and reactions, Marvin 17.21.0, ChemAxon (https://www.chemaxon.com).

Appendix A. Supplementary material

Supplementary data to this article can be found online at https://doi.org/10.1016/j.ejpb.2022.03.009.

References

[1] J.H. Jones, A short guide to abbreviations and their use in peptide science, J. Peptide Sci.: An Official Publication Eur. Peptide Soc. 5 (1999) 465–471.
[2] WHO, Global Tuberculosis Report 2020, in, World Health Organization, 2020.
[3] WHO, Global tuberculosis report 2019, in, World Health Organization, 2019.
[4] S. Chetty, M. Ramesh, A. Singh-Pillay, M.E. Soliman, Recent advancements in the development of anti-tuberculosis drugs, Bioorg. Med. Chem. Lett. 27 (2017) 370–386.
[5] K. Pauk, I. Zadrazilova, A. Imramovsky, J. Vinsova, M. Pokorna, M. Masarikova, A. Cizek, J. Jampilek, New derivatives of salicylamides: Preparation and antimicrobial activity against various bacterial species, Bioorg. Med. Chem. 21 (2013) 6574–6581.
[6] J.L. Zhang, H.F. Si, X.F. Shang, X.K. Zhang, B. Li, X.Z. Zhou, J.Y. Zhang, New life for an old drug: *In vitro* and *in vivo* effects of the anthelmintic drug niclosamide against *Toxoplasma gondii* RH strain, International journal for parasitology, Drugs Resistance 9 (2019) 27–34.
[7] E. Spaczynska, A. Mrozek-Wilczkiewicz, K. Malarz, J. Kos, T. Gonec, M. Oravec, R. Gawecki, A. Bak, J. Dohanosova, I. Kapustikova, T. Liptaj, J. Jampilek, R. Musiol, Design and synthesis of anticancer 1-hydroxynaphthalene-2-carboxanilides with a p53 independent mechanism of action, Sci. Rep. 9 (2019) 6387.
[8] J. Zhou, B. Jin, Y. Jin, Y. Liu, J. Pan, The antihelminthic drug niclosamide effectively inhibits the malignant phenotypes of uveal melanoma *in vitro* and *in vivo*, Theranostics 7 (6) (2017) 1447–1462.
[9] M.J. Macielag, J.P. Demers, S.A. Fraga-Spano, D.J. Hlasta, S.G. Johnson, R. M. Kanojia, R.K. Russell, Z. Sui, M.A. Weidner-Wells, H. Werblood, B.D. Foleno, R.M. Goldschmidt, M.J. Loeloff, G.C. Webb, J.F. Barrett, Substituted salicylanilides as inhibitors of two-component regulatory systems in bacteria, J. Med. Chem. 41 (16) (1998) 2939–2945.
[10] N. Dasgupta, V. Kapur, K.K. Singh, T.K. Das, S. Sachdeva, K. Jyothisri, J.S. Tyagi, Characterization of a two-component system, *devR-devS*, of *Mycobacterium tuberculosis*, Tubercle Lung Disease: The Official J. Int. Union against Tuberculosis Lung Dis. 80 (3) (2000) 141–159.
[11] M. Kratky, E. Novotna, S. Saxena, P. Yogeeswari, D. Sriram, M. Svarcova, J. Vinsova, Salicylanilide diethyl phosphates as potential inhibitors of some mycobacterial enzymes, TheScientificWorldJournal 2014 (2014), 703053.

[12] M. Krátký, J. Vinšová, E. Novotná, J. Stolaříková, Salicylanilide pyrazinoates inhibit *in vitro* multidrug-resistant *Mycobacterium tuberculosis* strains, atypical mycobacteria and isocitrate lyase, European journal of pharmaceutical sciences : official journal of the European Federation for, Pharmaceutical Sci. 53 (2014) 1–9.
[13] M. Kratky, M. Volkova, E. Novotna, F. Trejtnar, J. Stolarikova, J. Vinsova, Synthesis and biological activity of new salicylanilide N, N-disubstituted carbamates and thiocarbamates, Bioorganic Medicinal Chem. 22 (2014) 4073–4082.
[14] M. Kratky, J. Vinsova, Advances in mycobacterial isocitrate lyase targeting and inhibitors, Curr. Med. Chem. 19 (2012) 6126–6137.
[15] M. Kratky, J. Vinsova, E. Novotna, J. Mandikova, V. Wsol, F. Trejtnar, V. Ulmann, J. Stolarikova, S. Fernandes, S. Bhat, J.O. Liu, Salicylanilide derivatives block *Mycobacterium tuberculosis* through inhibition of isocitrate lyase and methionine aminopeptidase, Tuberculosis (Edinb) 92 (2012) 434–439.
[16] J.P. Boyce, M.E. Brown, W. Chin, J.N. Fitzner, R.J. Paxton, M. Shen, T. Stevens, M.F. Wolfson, C.D. Wright, Identification of 14-3-3zeta by chemical affinity with salicylanilide inhibitors of interleukin-12p40 production, Bioconjug. Chem. 19 (2008) 1775–1784.
[17] M.E. Brown, J.N. Fitzner, T. Stevens, W. Chin, C.D. Wright, J.P. Boyce, Salicylanilides: selective inhibitors of interleukin-12p40 production, Bioorg. Med. Chem. 16 (2008) 8760–8764.
[18] H. Terada, S. Goto, K. Yamamoto, I. Takeuchi, Y. Hamada, K. Miyake, Structural requirements of salicylanilides for uncoupling activity in mitochondria: quantitative analysis of structure-uncoupling relationships, BBA 936 (3) (1988) 504–512.
[19] I.Y. Lee, T.D. Gruber, A. Samuels, M. Yun, B. Nam, M. Kang, K. Crowley, B. Winterroth, H.I. Boshoff, C.E. Barry 3rd, Structure-activity relationships of antitubercular salicylanilides consistent with disruption of the proton gradient *via* proton shuttling, Bioorg. Med. Chem. 21 (2013) 114–126.
[20] S. Chakraborty, T. Gruber, C.E. Barry 3rd, H.I. Boshoff, K.Y. Rhee, *Para*-aminosalicylic acid acts as an alternative substrate of folate metabolism in *Mycobacterium tuberculosis*, Science 339 (2013) 88–91.
[21] J. Zheng, E.J. Rubin, P. Bifani, V. Mathys, V. Lim, M. Au, J. Jang, J. Nam, T. Dick, J.R. Walker, K. Pethe, L.R. Camacho, *para*-Aminosalicylic acid is a prodrug targeting dihydrofolate reductase in *Mycobacterium tuberculosis*, J. Biological Chem. 288 (2013) 23447–23456.
[22] A. Bermingham, J.P. Derrick, The folic acid biosynthesis pathway in bacteria: evaluation of potential for antibacterial drug discovery, BioEssays : News Rev. Mol., Cellular Dev. Biol. 24 (2002) 637–648.
[23] N.F. Kamaruzzaman, S. Kendall, L. Good, Targeting the hard to reach: challenges and novel strategies in the treatment of intracellular bacterial infections, Br. J. Pharmacol. 174 (2017) 2225–2236.
[24] J. Pieters, J. Gatfield, Hijacking the host: survival of pathogenic mycobacteria inside macrophages, Trends Microbiol. 10 (2002) 142–146.
[25] C.J. Queval, R. Brosch, R. Simeone, The Macrophage: A Disputed Fortress in the Battle against *Mycobacterium tuberculosis*, Front. Microbiol. 8 (2017) 2284.
[26] E.P. Thi, U. Lambertz, N.E. Reiner, Sleeping with the enemy: how intracellular pathogens cope with a macrophage lifestyle, PLoS Pathog. 8 (2012), e1002551.
[27] Z.S. Bhat, M.A. Rather, M. Maqbool, H.U. Lah, S.K. Yousuf, Z. Ahmad, Cell wall: A versatile fountain of drug targets in *Mycobacterium tuberculosis*, Biomed. Pharmacotherapy = Biomedecine Pharmacotherapie 95 (2017) 1520–1534.
[28] C. Hoffmann, A. Leis, M. Niederweis, J.M. Plitzko, H. Engelhardt, Disclosure of the mycobacterial outer membrane: cryo-electron tomography and vitreous sections reveal the lipid bilayer structure, PNAS 105 (2008) 3963–3967.
[29] Y.B. Sutar, J.K. Mali, V.N. Telvekar, R.S. Rajmani, A. Singh, Transferrin conjugates of antitubercular drug isoniazid: Synthesis and *in vitro* efficacy, Eur. J. Med. Chem. 183 (2019), 111713.
[30] S. Majumdar, S.K. Basu, Killing of intracellular *Mycobacterium tuberculosis* by receptor-mediated drug delivery, Antimicrob. Agents Chemother. 35 (1991) 135–140.
[31] É. Kiss, D. Schnöller, K. Pribranská, K. Hill, C.B. Pénzes, K. Horváti, S. Bősze, Nanoencapsulation of Antitubercular Drug Isoniazid and Its Lipopeptide Conjugate, J. Dispersion Sci. Technol. 32 (2011) 1728–1734.
[32] K. Horvati, G. Mezo, N. Szabo, F. Hudecz, S. Bosze, Peptide conjugates of therapeutically used antitubercular isoniazid-design, synthesis and antimycobacterial effect, J. Peptide Sci.: An Oficial Publication Eur. Peptide Soc. 15 (2009) 385–391.
[33] K. Horvati, B. Bacsa, N. Szabo, S. David, G. Mezo, V. Grolmusz, B. Vertessy, F. Hudecz, S. Bosze, Enhanced cellular uptake of a new, *in silico* identified antitubercular candidate by peptide conjugation, Bioconjug. Chem. 23 (2012) 900–907.
[34] K. Horvati, B. Bacsa, N. Szabo, K. Fodor, G. Balka, M. Rusvai, E. Kiss, G. Mezo, V. Grolmusz, B. Vertessy, F. Hudecz, S. Bosze, Antimycobacterial activity of peptide conjugate of pyridopyrimidine derivative against *Mycobacterium tuberculosis* in a series of *in vitro* and *in vivo* models, Tuberculosis (Edinb) 95 (Suppl 1) (2015) S207–S211.
[35] S. Bősze, F. Hudecz, Proteins and peptides for the immunodiagnosis and therapy of *Mycobacterium tuberculosis* infections, 40 (2016) 146-198.
[36] Z. Baranyai, M. Kratky, R. Vosatka, E. Szabo, Z. Senoner, S. David, J. Stolarikova, J. Vinsova, S. Bosze, *In vitro* biological evaluation of new antimycobacterial salicylanilide-tuftsin conjugates, Eur. J. Med. Chem. 133 (2017) 152–173.
[37] N.K. Jain, V. Mishra, N.K. Mehra, Targeted drug delivery to macrophages, Expert Opinion Drug Delivery 10 (2013) 353–367.
[38] A. Abraham, Z. Baranyai, G. Gyulai, E. Pari, K. Horvati, S. Bosze, E. Kiss, Comparative analysis of new peptide conjugates of antitubercular drug candidates-Model membrane and *in vitro* studies, Colloids and surfaces, B, Biointerfaces 147 (2016) 106–115.
[39] A.A. Amoscato, P.J. Davies, G.F. Babcock, K. Nishioka, Receptor-mediated internalization of tuftsin, Ann. N. Y. Acad. Sci. 419 (1983) 114–134.
[40] P. Gottlieb, E. Hazum, E. Tzehoval, M. Feldman, S. Segal, M. Fridkin, Receptor-mediated endocytosis of tuftsin by macrophage cells, Biochem. Biophys. Res. Commun. 119 (1984) 203–211.
[41] A.K. Agrawal, C.M. Gupta, Tuftsin-bearing liposomes in treatment of macrophage-based infections, Adv. Drug Deliv. Rev. 41 (2) (2000) 135–146.
[42] Z. Bar-Shavit, Y. Stabinsky, M. Fridkin, R. Goldman, Tuftsin-macrophage interaction: specific binding and augmentation of phagocytosis, J. Cell. Physiol. 100 (1) (1979) 55–62.
[43] P. Gottlieb, Y. Stabinsky, Y. Hiller, A. Beretz, E. Hazum, E. Tzehoval, M. Feldman, S. Segal, V. Zakuth, Z. Spirer, et al., Tuftsin receptors, Ann. N. Y. Acad. Sci. 419 (1983) 93–106.
[44] G.J. Prud'homme, Y. Glinka, Neuropilins are multifunctional coreceptors involved in tumor initiation, growth, metastasis and immunity, Oncotarget 3 (9) (2012) 921–939.
[45] H.-F. Guo, C.W. Vander Kooi, Neuropilin Functions as an Essential Cell Surface Receptor, J. Biol. Chem. 290 (49) (2015) 29120–29126.
[46] J.C. Nissen, D.L. Selwood, S.E. Tsirka, Tuftsin signals through its receptor neuropilin-1 *via* the transforming growth factor beta pathway, J. Neurochem. 127 (2013) 394–402.
[47] D. Bagnard, Neuropilin : from nervous system to vascular and tumor biology, Springer, US Adv. Exp. Med. Biol. (2002).
[48] S. Schellenburg, A. Schulz, D.M. Poitz, M.H. Muders, Role of neuropilin-2 in the immune system, Mol. Immunol. 90 (2017) 239–244.
[49] B. Chaudhary, Y.S. Khaled, B.J. Ammori, E. Elkord, Neuropilin 1: function and therapeutic potential in cancer, Cancer Immunol. Immunother. : CII 63 (2) (2014) 81–99.
[50] J.R.L. Wild, C.A. Staton, K. Chapple, B.M. Corfe, Neuropilins: expression and roles in the epithelium, Int. J. Exp. Pathol. 93 (2) (2012) 81–103.
[51] S. Roy, A.K. Bag, R.K. Singh, J.E. Talmadge, S.K. Batra, K. Datta, Multifaceted Role of Neuropilins in the Immune System: Potential Targets for Immunotherapy, Front. Immunol. 8 (2017) 1228.
[52] N.Y. Aung, R. Ohe, H. Meng, T. Kabasawa, S. Yang, T. Kato, M. Yamakawa, L. Tailleux, Specific Neuropilins Expression in Alveolar Macrophages among Tissue-Specific Macrophages, PLoS ONE 11 (2) (2016) e0147358.
[53] S. Hu, Z. Hu, J. Qin, C. Lin, X. Jiang, *In silico* analysis identifies neuropilin-1 as a potential therapeutic target for SARS-Cov-2 infected lung cancer patients, Aging 13 (2021) 15770–15784.
[54] E.J. Shim, E. Chun, H.R. Kang, S.H. Cho, K.U. Min, H.W. Park, Expression of semaphorin 3A and neuropilin 1 in asthma, J. Korean Med. Sci. 28 (2013) 1435–1442.
[55] C. Grandclement, C. Borg, Neuropilins: a new target for cancer therapy, Cancers 3 (2011) 1899–1928.
[56] M.A. von Wronski, N. Raju, R. Pillai, N.J. Bogdan, E.R. Marinelli, P. Nanjappan, K. Ramalingam, T. Arunachalam, S. Eaton, K.E. Linder, F. Yan, S. Pochon, M. F. Tweedle, A.D. Nunn, Tuftsin binds neuropilin-1 through a sequence similar to that encoded by exon 8 of vascular endothelial growth factor, J. Biol. Chem. 281 (2006) 5702–5710.
[57] T. Teesalu, K.N. Sugahara, V.R. Kotamraju, E. Ruoslahti, C-end rule peptides mediate neuropilin-1-dependent cell, vascular, and tissue penetration, Proceedings of the National Academy of Sciences of the United States of America, 106 (2009) 16157-16162.
[58] V.A. Najjar, Tuftsin, a natural activator of phagocyte cells: an overview, Ann. N. Y. Acad. Sci. 419 (1 Antineoplasti) (1983) 1–11.
[59] V.A. Najjar, K. Nishioka, "Tuftsin": a natural phagocytosis stimulating peptide, Nature 228 (1970) 672–673.
[60] M. Fridkin, V.A. Najjar, Tuftsin: its chemistry, biology, and clinical potential, Crit. Rev. Biochem. Mol. Biol. 24 (1) (1989) 1–40.
[61] A. Siebert, M. Gensicka-Kowalewska, G. Cholewinski, K. Dzierzbicka, Tuftsin - Properties and Analogs, Curr. Med. Chem. 24 (2017) 3711–3727.
[62] G. Mezo, A. Kalaszi, J. Remenyi, Z. Majer, A. Hilbert, O. Lang, L. Kohidai, K. Barna, D. Gaal, F. Hudecz, Synthesis, conformation, and immunoreactivity of new carrier molecules based on repeated tuftsin-like sequence, Biopolymers 73 (2004) 645–656.
[63] K.B. Bai, O. Lang, E. Orban, R. Szabo, L. Kohidai, F. Hudecz, G. Mezo, Design, synthesis, and *in vitro* activity of novel drug delivery systems containing tuftsin derivatives and methotrexate, Bioconjug. Chem. 19 (2008) 2260–2269.
[64] K. Horvati, G. Gyulai, A. Csampai, J. Rohonczy, E. Kiss, S. Bosze, Surface Layer Modification of Poly(d, l-lactic- co-glycolic acid) Nanoparticles with Targeting Peptide: A Convenient Synthetic Route for Pluronic F127-Tuftsin Conjugate, Bioconjug. Chem. 29 (2018) 1495–1499.
[65] J. Kopecek, P. Kopeckova, T. Minko, Z. Lu, HPMA copolymer-anticancer drug conjugates: design, activity, and mechanism of action, Eur. J. Pharm. Biopharm.: Official J. Arbeitsgemeinschaft fur Pharmazeutische Verfahrenstechnik e.V 50 (2000) 61–81.
[66] J.R. Kopecek, P., Strohalm, J., Ulbrich, K., Rihova, B., Chytry, V., Lloyd, J.B., Duncan, R., Synthetic polymeric drugs, in, Czech Academy of Science CAS Cancer Research Campaign Technology Ltd, United States, 1991.
[67] R. Edmondson, J.J. Broglie, A.F. Adcock, L. Yang, Three-dimensional cell culture systems and their applications in drug discovery and cell-based biosensors, Assay Drug Dev. Technol. 12 (2014) 207–218.
[68] A.J. Miller, J.R. Spence, *In Vitro* Models to Study Human Lung Development, Disease and Homeostasis, Physiology 32 (2017) 246–260.

[69] N. Karra, E.J. Swindle, H. Morgan, Drug delivery for traditional and emerging airway models, Organs-on-a-Chip 1 (2019), 100002.
[70] W.-M. Choi, P. Kopečková, T. Minko, J. Kopeček, Synthesis of HPMA Copolymer Containing Adriamycin Bound via an Acid-Labile Spacer and its Activity toward Human Ovarian Carcinoma Cells, Journal of Bioactive and Compatible Polymers 14 (1999) 447–456.
[71] J. Kopecek, P. Rejmanova, J. Strohalm, K. Ulbrich, B. Rihova, Vladimir Chytry, J. B. Lloyd, R. Duncan, Synthetic polymeric drugs, in, United States, 1991.
[72] K. Valko, Application of high-performance liquid chromatography based measurements of lipophilicity to model biological distribution, J. Chromatogr. A 1037 (2004) 299–310.
[73] E. Rutkowska, K. Pajak, K. Jozwiak, Lipophilicity–methods of determination and its role in medicinal chemistry, Acta Pol. Pharm. 70 (2013) 3–18.
[74] A.I. Fernandez-Llamazares, J. Adan, F. Mitjans, J. Spengler, F. Albericio, Tackling lipophilicity of peptide drugs: replacement of the backbone *N*-methyl group of cilengitide by *N*-oligoethylene glycol (N-OEG) chains, Bioconjug. Chem. 25 (2014) 11–17.
[75] A. Nalbandian, B.S. Yan, A. Pichugin, R.T. Bronson, I. Kramnik, Lung carcinogenesis induced by chronic tuberculosis infection: the experimental model and genetic control, Oncogene 28 (2009) 1928–1938.
[76] V. Cukic, The Association Between Lung Carcinoma and Tuberculosis, Medical archives 71 (2017) 212–214.
[77] M. Kratky, S. Bosze, Z. Baranyai, I. Szabo, J. Stolarikova, G. Paraskevopoulos, J. Vinsova, Synthesis and *in vitro* biological evaluation of 2-(phenylcarbamoyl) phenyl 4-substituted benzoates, Bioorg. Med. Chem. 23 (2015) 868–875.
[78] M. Kratky, S. Bosze, Z. Baranyai, J. Stolarikova, J. Vinsova, Synthesis and biological evolution of hydrazones derived from 4-(trifluoromethyl) benzohydrazide, Bioorg. Med. Chem. Lett. 27 (2017) 5185–5189.
[79] M. Kratky, O. Jandourek, Z. Baranyai, E. Novotna, J. Stolarikova, S. Bosze, J. Vinsova, Phenolic *N*-monosubstituted carbamates: Antitubercular and toxicity evaluation of multi-targeting compounds, Eur. J. Med. Chem. 181 (2019), 111578.
[80] M. Kratky, Z. Baranyai, S. Stepankova, K. Svrckova, M. Svarcova, J. Stolarikova, L. Horvath, S. Bosze, J. Vinsova, *N*-Alkyl-2-[4-(trifluoromethyl)benzoyl] hydrazine-1-carboxamides and Their Analogues: Synthesis and Multitarget Biological Activity, Molecules 25 (2020).
[81] V. Pflégr, L. Horváth, J. Stolaříková, A. Pál, J. Korduláková, S. Bősze, J. Vinšová, M. Krátký, Design and synthesis of 2-(2-isonicotinoylhydrazineylidene) propanamides as InhA inhibitors with high antitubercular activity, Eur. J. Med. Chem. 223 (2021) 113668, https://doi.org/10.1016/j.ejmech.2021.113668.
[82] S.G. Reed, C.F. Nathan, D.L. Pihl, P. Rodricks, K. Shanebeck, P.J. Conlon, K. H. Grabstein, Recombinant granulocyte/macrophage colony-stimulating factor activates macrophages to inhibit *Trypanosoma cruzi* and release hydrogen peroxide, Comparison with interferon gamma, J. Experimental Med. 166 (1987) 1734–1746.
[83] E.R. Stanley, Murine bone marrow-derived macrophages, Methods Mol. Biol. 5 (1990) 299–302.
[84] S.H.E. Kaufmann, L. Peiser, P.J. Gough, T. Kodama, S. Gordon, Macrophage class A scavenger receptor-mediated phagocytosis of *Escherichia coli*: role of cell heterogeneity, microbial strain, and culture conditions in vitro, Infect. Immun. 68 (4) (2000) 1953–1963.
[85] R. Szabó, L. Peiser, A. Plüddemann, S. Bösze, S. Heinsbroek, S. Gordon, F. Hudecz, Uptake of Branched Polypeptides with Poly[l-Lys] Backbone by Bone-Marrow Culture-Derived Murine Macrophages: The Role of the Class A Scavenger Receptor, Bioconjug. Chem. 16 (2005) 1442–1450.
[86] P.D. Antonio, M. Lasalvia, G. Perna, V. Capozzi, Scale-independent roughness value of cell membranes studied by means of AFM technique, Biochimica et Biophysica Acta (BBA) -, Biomembranes 1818 (2012) 3141–3148.
[87] S. Bosze, F. Zsila, B. Biri-Kovacs, B. Szeder, Z. Majer, F. Hudecz, K. Uray, Tailoring Uptake Efficacy of HSV-1 gD Derived Carrier Peptides, Biomolecules 10 (2020).
[88] H.W. Ziegler-Heitbrock, E. Thiel, A. Futterer, V. Herzog, A. Wirtz, G. Riethmuller, Establishment of a human cell line (Mono Mac 6) with characteristics of mature monocytes, Int. J. Cancer 41 (1988) 456–461.
[89] W. Erl, C. Weber, C. Wardemann, P.C. Weber, Adhesion properties of Mono Mac 6, a monocytic cell line with characteristics of mature human monocytes, Atherosclerosis 113 (1995) 99–107.
[90] E.L. Wright, D.C. Quenelle, W.J. Suling, W.W. Barrow, Use of Mono Mac 6 human monocytic cell line and J774 murine macrophage cell line in parallel antimycobacterial drug studies, Antimicrob. Agents Chemother. 40 (1996) 2206–2208.
[91] H. Tomioka, K. Sato, H. Kajitani, T. Akaki, S. Shishido, Comparative antimicrobial activities of the newly synthesized quinolone WQ-3034, levofloxacin, sparfloxacin, and ciprofloxacin against *Mycobacterium tuberculosis* and *Mycobacterium avium* complex, Antimicrob. Agents Chemother. 44 (2000) 283–286.
[92] D. Jonas, I. Engels, F.D. Daschner, U. Frank, The effect of azithromycin on intracellular *Legionella pneumophila* in the Mono Mac 6 cell line at serum concentrations attainable *in vivo*, J. Antimicrob. Chemother. 46 (2000) 385–390.
[93] D. Jonas, I. Engels, C. Friedhoff, B. Spitzmuller, F.D. Daschner, U. Frank, Efficacy of moxifloxacin, trovafloxacin, clinafloxacin and levofloxacin against intracellular *Legionella pneumophila*, J. Antimicrob. Chemother. 47 (2001) 147–152.
[94] M.W. Valderas, W.W. Barrow, Establishment of a method for evaluating intracellular antibiotic efficacy in *Brucella abortus*-infected Mono Mac 6 monocytes, J. Antimicrob. Chemother. 61 (2008) 128–134.
[95] K. Horvati, B. Bacsa, E. Kiss, G. Gyulai, K. Fodor, G. Balka, M. Rusvai, E. Szabo, F. Hudecz, S. Bosze, Nanoparticle encapsulated lipopeptide conjugate of antitubercular drug isoniazid: *in vitro* intracellular activity and *in vivo* efficacy in a Guinea pig model of tuberculosis, Bioconjug. Chem. 25 (2014) 2260–2268.
[96] N. Kósa, Á. Zolcsák, I. Voszka, G. Csík, K. Horváti, L. Horváth, S. Bősze, L. Herenyi, Comparison of the Efficacy of Two Novel Antitubercular Agents in Free and Liposome-Encapsulated Formulations, Int. J. Mol. Sci. 22 (5) (2021) 2457, https://doi.org/10.3390/ijms22052457.
[97] Z. Baranyai, B. Biri-Kovács, M. Krátký, B. Szeder, M.L. Debreczeni, J. Budai, B. Kovács, L. Horváth, E. Pári, Z. Németh, L. Cervenak, F. Zsila, E. Méhes, É. Kiss, J. Vinšová, S. Bősze, Cellular Internalization and Inhibition Capacity of New Anti-Glioma Peptide Conjugates: Physicochemical Characterization and Evaluation on Various Monolayer- and 3D-Spheroid-Based *in Vitro* Platforms, J. Med. Chem. 64 (2021) 2982–3005.
[98] D. Dube, M. Gupta, S.P. Vyas, Nanocarriers for Drug Targeting to Macrophages: Emerging Options for a Therapeutic Need, Proc. Natl. Acad. Sci., India, Sect. B Biol. Sci. 82 (S1) (2012) 151–165.
[99] T. Dutta, M. Garg, N.K. Jain, Targeting of efavirenz loaded tuftsin conjugated poly (propyleneimine) dendrimers to HIV infected macrophages *in vitro*, European journal of pharmaceutical sciences : official journal of the European Federation for, Pharm. Sci. 34 (2-3) (2008) 181–189.
[100] M. Fridkin, H. Tsubery, E. Tzehoval, A. Vonsover, L. Biondi, F. Filira, R. Rocchi, Tuftsin-AZT conjugate: potential macrophage targeting for AIDS therapy, J. Peptide Sci.: An Official Publication Eur. Peptide Soc. 11 (2005) 37–44.
[101] J.M. Irache, H.H. Salman, C. Gamazo, S. Espuelas, Mannose-targeted systems for the delivery of therapeutics, Expert Opinion Drug Delivery 5 (6) (2008) 703–724.
[102] U. Kauscher, B.J. Ravoo, Mannose-decorated cyclodextrin vesicles: The interplay of multivalency and surface density in lectin-carbohydrate recognition, Beilstein J. Org. Chem. 8 (2012) 1543–1551.
[103] M.F. Tweedle, Peptide-targeted diagnostics and radiotherapeutics, Acc. Chem. Res. 42 (7) (2009) 958–968.
[104] E. Wong, S. Bennett, B. Lawrence, T. Fauconnier, L.F. Lu, R.A. Bell, J. R. Thornback, D. Eshima, Tuftsin receptor-binding peptide labeled with technetium: chemistry and preliminary *in vitro* receptor-binding study, Inorg. Chem. 40 (2001) 5695–5700.
[105] J. Shao, J.P. Tam, Unprotected Peptides as Building Blocks for the Synthesis of Peptide Dendrimers with Oxime, Hydrazone, and Thiazolidine Linkages, J. Am. Chem. Soc. 117 (14) (1995) 3893–3899.
[106] J.P. Tam, Y.A. Lu, C.F. Liu, J. Shao, Peptide synthesis using unprotected peptides through orthogonal coupling methods. Proc. Natl. Acad. Sci. U.S.A. 92 (26) (1995) 12485–12489.
[107] S. Hiraki, M. Miyai, T. Seto, T. Tamura, Y. Watanabe, S. Ozawa, H. Ikeda, Y. Nakata, T. Ohnoshi, I. Kimura, Establishment of human continuous cell lines from squamous cell, adeno- and small cell carcinoma of the lung and the results of hetero-transplantation, Haigan 22 (1) (1982) 53–58.
[108] T. Mitsudomi, S.M. Steinberg, M.M. Nau, D. Carbone, D. D'Amico, S. Bodner, H. K. Oie, R.I. Linnoila, J.L. Mulshine, J.D. Minna, et al., p53 gene mutations in non-small-cell lung cancer cell lines and their correlation with the presence of ras mutations and clinical features, Oncogene 7 (1992) 171–180.
[109] J. Fogh, J.M. Fogh, T. Orfeo, One hundred and twenty-seven cultured human tumor cell lines producing tumors in nude mice, J. Natl Cancer Inst. 59 (1977) 221–226.
[110] J. Fogh, G. Trempe, in: Human Tumor Cells *in Vitro*, Springer US, Boston, MA, 1975, pp. 115–159, https://doi.org/10.1007/978-1-4757-1647-4_5.
[111] M.H. Larsen, K. Biermann, W.R. Jacobs Jr., Laboratory Maintenance of *Mycobacterium tuberculosis*, Curr. Protocols Microbiol. 6 (1) (2007). Chapter 10.
[112] L. Sula, T.K. Sundaresan, Who Co-Operative Studies on a Simple Culture Technique for the Isolation of *Mycobacteria*. 1. Preparation, Lyophilization and Reconstitution of a Simple Semi-Synthetic Concentrated Liquid Medium; Culture Technique; Growth Pattern of Different Mycobacteria, Bull. World Health Organ. 29 (1963) 589–606.
[113] L. Sula, T.K. Sundaresan, Who Co-Operative Studies on a Simple Culture Technique for the Isolation of *Mycobacteria*. 2. Comparison of the Efficacy of Lyophilized Liquid Medium with That of Loewenstein-Jensen (L-J) Medium, Bull. World Health Organ. 29 (1963) 607–625.
[114] E. Vavríková, J. Mandíková, F. Trejtnar, K. Horváti, S. Bősze, J. Stolaríková, J. Vinšová, Cytotoxicity decreasing effect and antimycobacterial activity of chitosan conjugated with antituberculotic drugs, Carbohyd. Polym 83 (2011) 1901–1907.
[115] E. Vavrikova, S. Polanc, M. Kocevar, K. Horvati, S. Bosze, J. Stolarikova, K. Vavrova, J. Vinsova, New fluorine-containing hydrazones active against MDR-tuberculosis, Eur. J. Med. Chem. 46 (2011) 4937–4945.
[116] E. Vavrikova, S. Polanc, M. Kocevar, J. Kosmrlj, K. Horvati, S. Bosze, J. Stolarikova, A. Imramovsky, J. Vinsova, New series of isoniazid hydrazones linked with electron-withdrawing substituents, Eur. J. Med. Chem. 46 (2011) 5902–5909.
[117] M. Kratky, J. Vinsova, V. Buchta, K. Horvati, S. Bosze, J. Stolarikova, New amino acid esters of salicylanilides active against MDR-TB and other microbes, Eur. J. Med. Chem. 45 (2010) 6106–6113.
[118] Z. Baranyai, M. Kratky, J. Vinsova, N. Szabo, Z. Senoner, K. Horvati, J. Stolarikova, S. David, S. Bosze, Combating highly resistant emerging pathogen *Mycobacterium abscessus* and *Mycobacterium tuberculosis* with novel salicylanilide esters and carbamates, Eur. J. Med. Chem. 101 (2015) 692–704.
[119] E. Loewenstein, Die Zuchtung der Tuberkelbazillen aus dem stroemenden, Blute Zentralbl. Bakteriol. Parasitenkd. Infektionskr. Hyg. Abt. 1 Orig 120 (1931).

[120] K.A. Jensen, Reinzuchtung und Typenbestimmung von Tuberkelbazillenstammen, Zentralbl. Bakteriol. Parasitenkd. Infektionskr. Hyg. Abt. I Orig 125 (1932).
[121] T. Mosmann, Rapid colorimetric assay for cellular growth and survival: application to proliferation and cytotoxicity assays, J. Immunol. Methods 65 (1-2) (1983) 55–63.
[122] T.F. Slater, B. Sawyer, U. Sträuli, Studies on Succinate-Tetrazolium Reductase Systems. Iii. Points of Coupling of Four Different Tetrazolium Salts, BBA 77 (1963) 383–393.
[123] Y. Liu, D.A. Peterson, H. Kimura, D. Schubert, Mechanism of cellular 3-(4,5-dimethylthiazol-2-yl)-2,5-diphenyltetrazolium bromide (MTT) reduction, J. Neurochem. 69 (2) (1997) 581–593.
[124] A. Kapus, S. Grinstein, S. Wasan, R. Kandasamy, J. Orlowski, Functional characterization of three isoforms of the Na^+/H^+ exchanger stably expressed in Chinese hamster ovary cells. ATP dependence, osmotic sensitivity, and role in cell proliferation, J. Biol. Chem. 269 (38) (1994) 23544–23552.
[125] H. Schägger, Tricine-SDS-PAGE, Nat. Protoc. 1 (1) (2006) 16–22.
[126] E. Orban, G. Mezo, P. Schlage, G. Csik, Z. Kulic, P. Ansorge, E. Fellinger, H. M. Moller, M. Manea, *In vitro* degradation and antitumor activity of oxime bond-linked daunorubicin-GnRH-III bioconjugates and DNA-binding properties of daunorubicin-amino acid metabolites, Amino Acids 41 (2011) 469–483.
[127] E. Mehes, D. Mornet, V. Jancsik, Subcellular localization of components of the dystrophin glycoprotein complex in cultured retinal muller glial cells, Acta Biol. Hung. 54 (2003) 241–252.
[128] R.M. Mège, N. Ishiyama, Integration of cadherin adhesion and cytoskeleton at adherens junctions, Cold Spring Harbor Perspect. Biol. 9 (5) (2017) a028738, https://doi.org/10.1101/cshperspect.a028738.